surrounding tissues and is supported mainly by the flexible lead wires and the nerve, the weight of the insulator mass may exert great mechanical stress on the nerve.

To avoid the unnecessary mechanical stress on the nerve, the cured insulator should have as light a mass as possible. With an appropriate viscosity, an insulator solution dropped on the electrode tips would adhere to the electrode tips and the nerve for a while. If insulator solution could be cured with proper timing, the cured insulator would be able to fix the electrode tips to the nerve in a small mass. This method would also make cavity formation unnecessary.

Photopolymerization has several advantages such as spatial and temporal control of the polymerization process, fast curing rate at room temperature, ease of fashioning, and minimal heat production [3,4]. Recent in vivo studies have indicated that the photo-induced curing systems can be applied to many biological systems without reaction. They include photocured endocapsular lens replacement for cataract treatment [5]; visible light-cured dental restorative materials [6] and orthopedic materials [7]; and photo-cured hydrogels used in angioplasty to promote better healing [8], tissue adhesion [9], and tissue engineered matrix formation [10].

In this study, a novel photocurable material was designed as an in vivo insulator material to record autonomic nerve activity. The material is basically a mixture of photo-crosslinkable bisacrylated alkyl monomer and Vaseline that is used for viscosity control. Camphorquinone (CQ), which has been applied in visible-light-curable dental resin composites for many years, is used as the polymerization photoinitiator. The insulator material was examined in terms of viscosity, photocrosslinking and insulation characteristics. This novel insulator was also applied in vivo for recording autonomic nerve activity in an acute stage experiment.

2. Materials and methods

2.1. Materials

White petrolatum (Vaseline), CQ and other chemicals were obtained from Wako Pure Chemical Industry, Ltd. (Osaka, Japan). All chemicals used were reagent grade and were used without further purification. 1,12-dodecanediol diacrylate (DDA) and dodecanol monoacrylate (DMA) were prepared by acrylation of 1,12-dodecanediol or dodecanol with acryloyl chloride in dichloromethane solution with a small amount of triethylamine. The resulting DDA and DMA were isolated and purified by column chromatography (silica gel 60, elution chloroform).

2.2. Preparation of photocurable insulator material and its photoirradiation

Photocurable insulator materials were prepared by mixing Vaseline, DDA and a small amount of CQ with or without DMA (Table 1). The typical composition of the photocurable insulator material for nerve activity recording was Vaseline and DDA (50:50 wt%) together with CQ at 0.25 wt%. Photoirradiation was conducted with a commercial halogen lamp (Power Light, Tokuso Co., Tokyo, Japan) commonly used in many current dental applications.

2.3. Viscosity and strength measurements

The viscosity of the photocurable insulator material was measured with a viscometer (R-105, Tokisangyo Co., Ltd., Tokyo, Japan). The compressive strength of the photocured insulator (i.e., the solid obtained after photoirradiation of the photocurable insulator material) of each composition was measured by a rheometer (RE-3305, Yamaden, Tokyo, Japan), which equipped with a 5-mm diameter rod-like Teflon probe and a sample stage, and measures the distance traversed by the probe into a given material as a function of the force applied. The photocured insulator $\approx$5 mm in thickness was placed on the sample stage of the rheometer. The center of the sample was continuously compressed by the probe at a rate of 0.5 mm/s at 25°C. The compressive force, P (in Pa), was determined as $P=(A\times 980)/(10\times S)$, where A (in g) and S (in cm^2) denote the load

Table 1
Compositions of photocurable insulators and their crosslinking characteristics

Composition (weight ratio)			Viscosity[b] (Pa s)	Irradiation time (min)	Compressive force[c] (kPa)
Vaseline	Macromer[a]				
	DDA	DMA			
100	0	0	2.2	2	4.7
90	10	0	1.4	2	5.8
80	20	0	0.77	2	6.1
70	30	0	0.51	2	28.8
60	40	0	0.26	2	122.4
50	50	0	0.18	0	0.5
50	50	0	NM	1	155.5
50	50	0	NM	2	321.6
50	40	10	NM	2	196.6
50	30	20	NM	2	142.2
50	20	30	NM	2	44.0
50	10	40	NM	2	10.6

[a] Containing CQ (0.5 wt% of macromer weight).
[b] Measured at 25°C before curing.
[c] Per mm deformation.
NM: not measured.

per mm sample deformation and contact area of the probe, respectively.

2.4. Impedance measurement

The impedance is the total opposition by a given material to an alternating current (AC) and is dependent on the frequency of AC. High impedance values are required for insulation of the electrodes and nerve. We measured the impedance of saline, Vaseline, silicone glue (Semicosil 932, Wacker silicones, USA), and photocurable insulator material at 25°C in the frequency range from 1 Hz to 100 kHz using an impedance meter (LCR HiTester, Hioki, Nagano, Japan). Each material was packed into a custom-made cylindrical cuvette (5 cm in length and 0.18 cm^2 in cross-sectional area) with 4 stainless steel electrodes (placed at intervals of 1.11 cm). The cuvette was translucent and the photocurable insulator material was cured by photoirradiation after packing. The external two electrodes were excited by AC so that the potential between the internal two electrodes was 0.1 or 0.5 V. The impedance was calculated from the current measured through the material. The measured impedance was converted into the impedance value for the material of 1 mm in length and 10 mm^2 in cross-sectional area, assuming actual application to the autonomic nerve activity recording.

2.5. Surgical preparations

Animals were cared in accordance with the Guiding Principles for the Care and Use of Animals in the Field of Physiological Sciences approved by the Physiological Society of Japan. Three Japanese white rabbits were anesthetized with intravenous injection of pentobarbital sodium via the ear vein (35 mg/kg). The animals were intubated through tracheotomy and mechanically ventilated with oxygen-enriched room air. Supplemental anesthetic was injected as necessary (5 mg/kg) to maintain an appropriate depth of anesthesia. Arterial pressure (AP) was recorded from a catheter inserted into the right femoral artery. A double-lumen catheter was inserted into the right femoral vein for later drug administration. With the animal in the lateral position, the left renal sympathetic nerve was exposed retroperitoneally through a flank incision. A pair of urethane-coated, stainless steel wire electrodes (0.08 mm in diameter) (Unique Medical, Tokyo, Japan) were attached to the renal nerve and fixed with the photocurable insulator solution of typical composition. Next, with the animal in supine position, the left aortic depressor nerve (ADN) was exposed through a midline cervical incision. Another pair of stainless steel wire electrodes were attached to the depressor nerve and fixed with the photocurable insulator material. The nerve signals were preamplified and band-pass filtered at 150 Hz–1 kHz using difference amplifiers (MEG-6100, Nihon Kohden, Japan) to record the aortic depressor nerve activity (ADNA) and renal sympathetic nerve activity (RSNA). The integrated ADNA (iADNA) and integrated RSNA (iRSNA) were obtained by full-wave rectification followed by low-pass filtering at 30 Hz. All signals were digitized and stored on a hard disk of a laboratory computer at a sampling rate of 5 kHz using a 12-bit analog-to-digital converter (AD12-16U(PCI)E, Contec, Japan). Pancuronium bromide (0.3 mg/kg) was administered to prevent contamination of muscular activity in the ADNA and RSNA recordings. Body temperature was maintained at 38°C with a heating pad.

2.6. Drug administration

To examine the ADNA and RSNA responses to changes in AP, glycerin trinitrate (GTN; 10 μg/kg, i.v.) or phenylephrine (10 μg/kg, i.v.) was injected. The GTN administration was expected to decrease AP, resulting in a decrease in ADNA and a reflex increase in RSNA. The phenylephrine administration was expected to induce nerve activity responses opposite to GTN.

3. Results and discussion

3.1. Formulation of photocurable insulator material and photocrosslinking

The novel photocurable insulator material was composed of Vaseline and difunctional long alkyl chain monomer (DDA) with or without monofunctional long alkyl chain monomer (DMA). A small amount of CQ was added to the mixture as a photoinitiator. A series of mixtures with different compositions were prepared (Table 1). All the mixtures gave viscous fluids and were milky at 25°C but transparent at 37°C. The viscosity of the mixtures decreased markedly with an increase in content of macromer (Table 1). The viscosity at a 50 wt% of macromer was about 0.18 Pa s, similar to that of liquid paraffin (ca. 0.2 Pa s).

A mixture of Vaseline, DDA and CQ with or without DMA, which were not subjected to degassing to remove oxygen, was cured upon a short period of photoirradiation (1–2 min), whereas Vaseline alone did not even in the presence of CQ. Therefore, the solidification was a result of crosslinking of DDA by radical polymerization initiated by CQ. The degree of crosslinking was estimated from the compressive force of the resulting solid. The load-deformation relationships of the solid are shown in Fig. 1. In mixtures containing DDA at concentrations below 20 wt%, little increase in load was observed in response to deformation. The slopes of the load-deformation curves increased with an increase in concentration of DDA. The compressive forces per mm

deformation calculated from the slopes are summarized in Table 1. The force increased with an increase in DDA concentration and/or increase in irradiation time. When a part of DDA was replaced by DMA, the compressive force of the produced solid decreased as the concentration of DMA increased.

3.2. Impedance property

Table 2 summarizes the impedance values of materials. The impedance value of saline at 10 kHz (66 Ω) approximated the theoretical resistance of saline (61 Ω, see Appendix A), indicating that the custom-made cuvette worked reasonably well. All of the photocured insulator, Vaseline, DDA and silicone glue showed impedance values > 1 MΩ in the frequency range up to 1 kHz. Although the impedance decreased at frequencies above 1 kHz, the decrease in the impedance would have little effect on the nerve activity recording, because the nerve activity was preamplified and band-pass filtered between 150 Hz and 1 kHz.

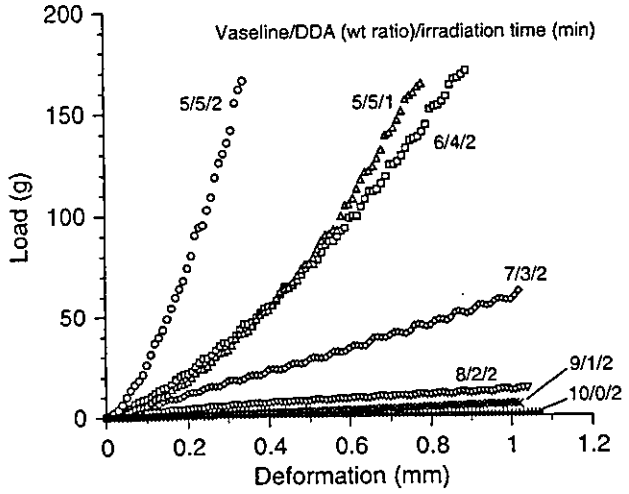

Fig. 1. Load-deformation relationships of various mixtures of Vaseline, 1,12-dodecanediol diacrylate (DDA). The mixtures contained camphorquinone (CQ) at 0.5 wt% of macromer weight. The wt ratio of Vaseline:DDA varied from 10:0 to 5:5. The photoirradiation time was either 1 or 2 min.

3.3. In vivo application

Since a mixture of Vaseline and DDA at 50:50 wt% together with CQ at 0.25 wt% had a viscosity appropriate for handling at room temperature and also exhibited good rigidity after photocuring, this mixture was tested for suitability as an in situ photocurable insulator material for recording autonomic nerve activities.

Fig. 2 depicts application of the photocurable insulator material to the ADNA recording. The ADN was isolated from surrounding tissue and hung by a pair of stainless steel wire electrodes. A small drop of the photocurable insulator material was applied around the electrode tips using a 23-gauge needle. Upon photoirradiation, the insulator material was crosslinked and the electrode tips were fixed on the nerve by the insulator coating. When subsequent application of saline around the insulator coating short-circuited the electrode tips, application and photoirradiation of the photocurable insulator material could be repeated. Finally, the stainless steel lead wires were loosened and sutured to the nearby muscular tissue to minimize mechanical stress on the nerve.

3.4. Nerve activity recordings

Fig. 3 shows a typical time series of AP, ADNA, iADNA, RSNA and iRSNA obtained 2 h after the completion of surgical preparations. ADNA and iADNA showed pulsatile activities corresponding to the pulsatile AP. In contrast, RSNA and iRSNA showed clustered activities associated with respiration. The pulse-synchronized activities were evident in the clustered activities of RSNA and iRSNA. The quality of nerve recording did not change perceivably from the initiation of nerve activity recording up to 2 h in all animals, suggesting that the insulation by the photocured insulator was stable.

Fig. 4 illustrates a typical time series of AP, iADNA, and iRSNA during pharmacological interventions. In order to focus on the slower changes than in Fig. 3, all signals were resampled at 0.1 Hz. Because the magnitude

Table 2
Modulus of material impedance corrected for 1-mm length and 10-mm^2 cross-sectional area (Ω)

	Photocurable Insulator[a,b]	Saline	Vaseline	DDA[c,b]	Silicone glue[b]
1 Hz	11.9 M	266	13.1 M	10.5 M	11.3 M
10 Hz	10.4 M	80	12.8 M	10.2 M	11.0 M
100 Hz	8.6 M	69	11.3 M	9.7 M	11.3 M
1 kHz	4.2 M	66	2.9 M	2.8 M	2.9 M
10 kHz	275 k	66	210 k	235 k	210 k
100 kHz	26 k	66	19 k	22 k	19 k

[a] Mixture of Vaseline, DDA, and CQ (50, 50, and 0.25 wt% of material, respectively).
[b] Measured after curing.
[c] Containing CQ (0.5 wt% of macromer).

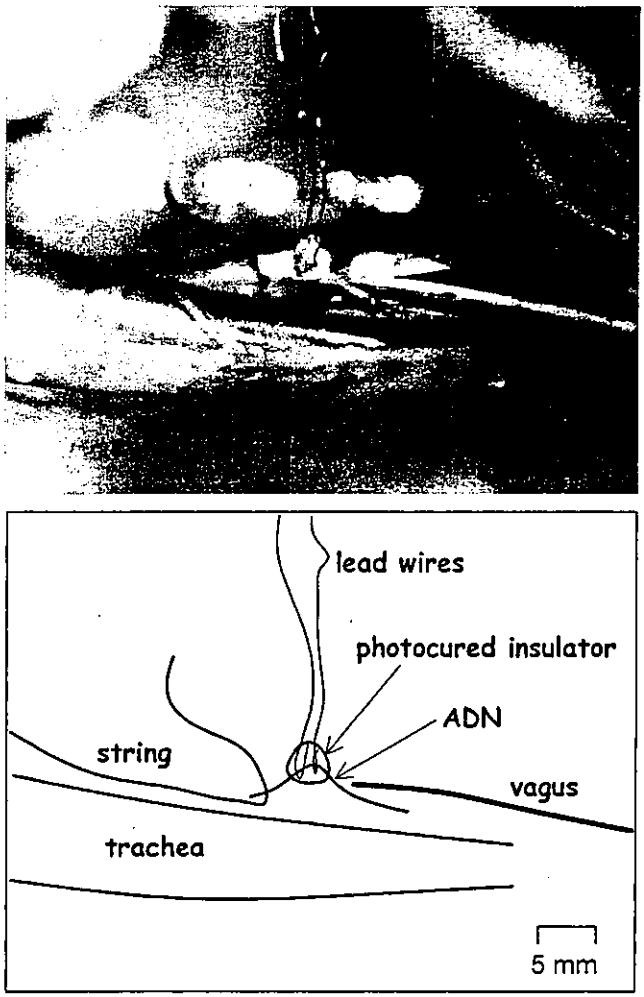

Fig. 2. Application of the photocurable insulator material to the left aortic depressor nerve (ADN).

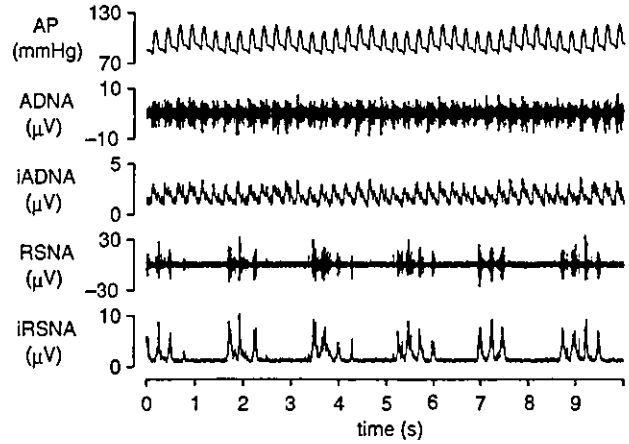

Fig. 3. Typical time series of arterial pressure (AP), aortic depressor nerve activity (ADNA), integrated ADNA (iADNA), renal sympathetic nerve activity (RSNA), and integrated RSNA (iRSNA).

of nerve activity depends on the resampling rate, iADNA and iRSNA are expressed in arbitrary units (a.u.). The GTN administration decreased AP, which decreased iADNA, and iRSNA was increased by the

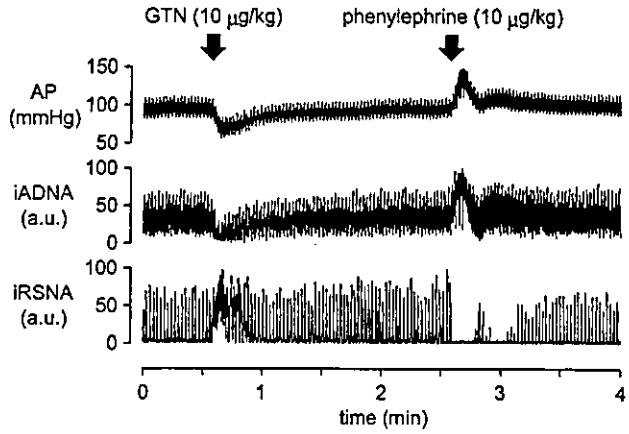

Fig. 4. Typical time series of AP, iADNA, and iRSNA in response to intravenous administrations of glycerin trinitrate (GTN) and phenylephrine.

negative feedback through the arterial baroreflex. On the other hand, the phenylephrine administration increased AP, and iADNA increased parallel to changes in AP, whereas iRSNA was shut down. These results suggest that the photocurable insulator material and the photocured insulator had no tissue toxicity, at least for the experimental period of the present study (i.e., 2 h). This period is sufficiently long for ordinary acute experiments.

4. Conclusion

We have developed a photocurable insulator material that can cover the electrode tips and nerve in situ in a very small mass. Using this insulator material in an in vivo experiment, the autonomic nerve activities were stably recorded at least in the acute stage of experimentation. The greatest advantage of the novel photocurable insulator material is that the material can be cured in a small mass, a few mm in diameter, and does not require a cavity around the recording site (Fig. 2). This feature is achieved by the appropriate viscosity of the insulator material before curing and the convenient curing procedure of photoirradiation at any desired timing. The small insulator mass would be beneficial for stable recording of autonomic nerve activity, because it minimizes the mechanical stress on the nerve induced by the weight and inertia of the insulator mass. Although further chronic experiments are required to validate the utility of the photocurable insulator material for long-term autonomic nerve activity recording, the photocurable insulator material may be an alternative to the addition-curing silicone glue.

Acknowledgements

This study was supported by Research Grants for Cardiovascular Diseases (9C-1, 11C-3, 11C-7) from the Ministry of Health and Welfare of Japan, by a Health Sciences Research Grant for Advanced Medical Technology and Human Genome, Tissue Engineering Food Biotechnology from the Ministry of Health, Labour and Welfare of Japan, by a Ground-Based Research Grant for the Space Utilization promoted by NASDA and Japan Space Forum, by Grant-in-Aid for Scientific Research (B-11694337, B-13450302, C-11680862, C-11670730) and Grant-in-Aid for Encouragement of Young Scientists (13770378) from the Ministry of Education, Science, Sports and Culture of Japan, and by the Program for Promotion of Fundamental Studies in Health Science from the Organization for Pharmaceutical Safety and Research.

Appendix A. Impedance of saline

Conductivity of 0.1-mol/dm^3 sodium chloride solution is 1.067/Ω m at 25°C. Given that saline contains 0.9 wt% of sodium chloride, the resistance [$R(\Omega)$] of saline for an 1-mm length and 10-mm^2 cross-sectional area can be calculated as follows:

$$R = \frac{0.001}{10 \times 0.001^2 \times 1.067} \times \frac{(23 + 35.45) \times 0.1}{1000 \times 0.009} = 60.9.$$

References

[1] Kawada T, Sato T, Shishido T, Inagaki M, Tatewaki T, Yanagiya Y, Sugimachi M, Sunagawa K. Summation of dynamic transfer characteristics of left and right carotid sinus baroreflexes in rabbits. Am J Physiol Heart Circ Physiol 1999;277:H857–65.

[2] Kawada T, Shishido T, Inagaki M, Tatewaki T, Zheng C, Yanagiya Y, Sugimachi M, Sunagawa K. Differential dynamic baroreflex regulation of cardiac and renal sympathetic nerve activities. Am J Physiol Heart Circ Physiol 2001;280:H1581–90.

[3] Nakayama Y, Matsuda T. Surface macromolecular architectural designs using photo-graft copolymerization based on photochemistry of benzyl N,N-diethyldithiocarbamate. Macromolecules 1996;29:8622–30.

[4] Nakayama Y, Ji-Youn K, Nishi S, Ueno H, Matsuda T. Development of high-performance stent: gelatinous photogel-coated stent that permits drug delivery and gene transfer. J Biomed Mater Res 2001;57:559–66.

[5] Grubbs RH, Coots RJ, Pine SH. Synthetic polymer for endocapsular lens replacement. US Patent 4,919,151, 1990.

[6] Anseth KS, Newman SM, Bowman CN. Polymeric dental composites: properties and reaction behavior of multimethacrylate dental restorations. Adv Polym Sci 1995;122:177–218.

[7] Anseth KS, Shastri VR, Langer R. Photopolymerizable degradable polyanhydrides with asteocompatibility. Nature Biotechnol 1999;17:156–9.

[8] Hill-West JL, Chowdhury SM, Slepian MJ, Hubbell JA. Inhibition of thrombosis and initial thickening by in situ photopolymerization of thin hydrogel barriers. Proc Natl Acad Sci USA 1994;91:5967–71.

[9] Nakayama Y, Matsuda T. Photocurable surgical tissue adhesive glues composed of photoreactive gelatin and poly(ethylene glycol) diacrylate. J Biomed Mater Res (Appl Biomater) 1999;48:511–21.

[10] Elisseeff J, Anseth K, Smis D, McIntosh W, Randolph M, Ranger R. Transdermal photopolymerization for minimally inveasive implantation. Proc Natl Acad Sci USA 1999;96:3104–7.

Biomaterial adherent macrophage apoptosis is increased by hydrophilic and anionic substrates *in vivo*

William G. Brodbeck*†, Jasmine Patel‡, Gabriela Voskerician‡, Elizabeth Christenson‡, Matthew S. Shive‡, Yasuhide Nakayama§, Takehisa Matsuda¶, Nicholas P. Ziats*‡, and James M. Anderson*†‡

Departments of *Pathology and ‡Biomedical Engineering, Case Western Reserve University, Cleveland, OH 44139; §Department of Bioengineering, National Cardiovascular Center, Osaka 562-0025, Japan; and ¶Department of Biomedical Engineering, Kyushu University, Fukuoka 812-8482, Japan

Edited by Robert Langer, Massachusetts Institute of Technology, Cambridge, MA, and approved June 10, 2002 (received for review March 4, 2002)

An *in vivo* rat cage implant system was used to identify potential surface chemistries that prevent failure of implanted biomedical devices and prostheses by limiting monocyte adhesion and macrophage fusion into foreign-body giant cells while inducing adherent-macrophage apoptosis. Hydrophobic, hydrophilic, anionic, and cationic surfaces were used for implantation. Analysis of the exudate surrounding the materials revealed no differences between surfaces in the types or levels of cells present. Conversely, the proportion of adherent cells undergoing apoptosis was increased significantly on anionic and hydrophilic surfaces (46 ± 3.7 and 57 ± 5.0%, respectively) when compared with the polyethylene terephthalate base surface. Additionally, hydrophilic and anionic substrates provided decreased rates of monocyte/macrophage adhesion and fusion. These studies demonstrate that biomaterial-adherent cells undergo material-dependent apoptosis *in vivo*, rendering potentially harmful macrophages nonfunctional while the surrounding environment of the implant remains unaffected.

The host foreign-body response ensues immediately after implantation of biomedical devices and prostheses. This response progresses through stages of inflammation and wound healing with different cell types as hallmark indicators of the particular stage of the reaction. Neutrophils and mononuclear cells immediately infiltrate the tissue–material interface and are associated with acute inflammation. Chronic inflammation is evident when the number of infiltrating neutrophils decrease and the local monocyte population adheres to the surface of the implant and differentiates into macrophages. Lymphocytes also become more predominant during the chronic phase of inflammation. The total number of infiltrating cells normally decreases as the inflammatory response resolves and the wound-healing process progresses to the formation of granulation tissue and subsequent fibrous encapsulation of the implanted material. Although formation of this foreign-body capsule is thought to be beneficial to the implant, cells already adherent to the surface eventually may cause failure of the device. These adherent cells consist of monocyte-derived macrophages, which may fuse into foreign-body giant cells (FBGCs) that concentrate degradative and phagocytic properties leading to structural and chemical damage of the implant (1, 2). Therefore, methods of effectively modulating the presence and activity of adherent monocytes/macrophages/FBGCs would enhance the *in vivo* lifetime of implanted devices.

The rat cage implant system is an *in vivo* model that focuses on the types and levels of infiltrating and adherent inflammatory cells on or surrounding the biomaterial after s.c. implantation. With such studies, although the presence and levels of acute or chronic cell types may indicate the overall response to an implanted device, very little information is available regarding the functional capabilities of the exudate or adherent-cell populations. This information is paramount for engineering surfaces that modify the presence and function of adherent monocytes, macrophages, and FBGCs. One such mechanism can be provided by the induction of apoptosis of biomaterial-adherent cells.

We have reported that biomaterial-adherent cell apoptosis is influenced by the chemistry of the surface of adhesion *in vitro* (3). Particular surface chemistries were chosen to represent a broad spectrum of biomaterial applications. In other studies, we have identified the detrimental apoptotic effects of fluid shear stress on biomaterial-adherent neutrophils, which may lead to increased susceptibility of cardiovascular prostheses to bacterial infection (4). Although the literature pertaining to biomaterial-related apoptosis is expanding rapidly, only limited numbers of studies have explored this topic *in vivo*. Honma and Hamasaki examined apoptotic FBGCs adherent to collagen sponges (5), but these studies lacked information with respect to the area surrounding the implant, i.e., the overall response to the material. Others have identified material- and time-dependent apoptosis of neutrophils contained within exudate (6); however, these studies focused on short-term analyses (2 days) and provided no information regarding the biomaterial-adherent cell population. Our *in vivo* studies were performed by using the rat cage implant system with examination of both adherent and exudate cells. We correlated the induction of adherent-cell apoptosis to possible alterations, if any, in the types and levels of cells present surrounding the implant, indicating the progression and resolution of the inflammatory response. Adherent-cell densities, rates of fusion, and levels of apoptosis as well as exudate cell types, levels, and rates of apoptosis were determined. Importantly, these studies demonstrate that, *in vivo*, hydrophilic and anionic surfaces promote decreased monocyte adhesion and increased proportions of adherent apoptotic monocytes/macrophages, potentially reducing the risk of implant damage and failure caused by these cells.

Materials and Methods

Surface Preparation. Biomaterial surfaces displaying distinct surface chemistries were prepared with a custom-designed semiautomatic apparatus for laboratory-scale mass production as described (7, 8). The surfaces consisted of polyethylene terephthalate film coated with poly(benzyl *N,N*-diethyldithiocarbamate-co-styrene) (BDEDTC) and either polyacrylamide, sodium salt of poly(acrylic acid), or methiodide of poly(dimethylaminopropyl-acrylamide) were photograft-copolymerized to the BDEDTC surface. These surfaces were characterized in other studies (3) and are considered slightly hydrophobic, hydrophobic, hydrophilic, anionic, and cationic, respectively (Table 1).

This paper was submitted directly (Track II) to the PNAS office.

Abbreviation: FBGC, foreign-body giant cell.

†To whom reprint requests may be addressed at: Institute of Pathology, Room 306, Case Western Reserve University School of Medicine, Cleveland OH 44106. E-mail: jma6@po.cwru.edu or wgb2@po.cwru.edu.

Table 1. Surface properties

Surface	Chemical property	Advancing water contact angle
PET base surface	Slightly hydrophobic	47.6 ± 2.1
BDEDTC-coated surface	Hydrophobic	83.3 ± 1.7
PAAm	Hydrophilic	28.4 ± 3.2
PAANa	Anionic	25.9 ± 2.0
DMAPAAmMel	Cationic	28.0 ± 1.1

PET, polyethylene terephthalate; BDEDTC, poly(benzyl *N,N*-diethyldithiocarbamate-co-styrene; PAAm, polyacrylamide; PAANa, sodium salt of poly(acrylic acid); DMAPAAmMel, poly(dimethylaminopropyl acrylamide).

Rat Cage Implant System. Implants were performed as described (9, 10). Briefly, surfaces were placed in surgical-grade stainless steel wire mesh cages (1.5 cm in length, 0.5 cm in diameter, 0.25-mm wire diameter, and 0.8-mm opening width with 58% open area) and sterilized with ethylene oxide. Cages containing surfaces were implanted s.c. in the backs, at the level of the panniculus carnosus, of anesthetized 3-month-old 250–300 g female Sprague–Dawley rats according to National Institutes of Health guidelines.

Exudate Cell Analyses. On days 7, 14, and 21, 300–1,000 μl of exudate surrounding the implant within the cages were drawn before explantation. One half of the exudate was processed for total leukocyte and differential cell counting (described in ref. 10), and the other half was stained for apoptosis markers for analysis by flow cytometry. Collected cells were pelleted and washed twice before staining with annexin V-FITC and propidium iodide (R & D Systems) according to manufacturer instructions. The double-stained cells then were washed again and analyzed immediately by flow cytometry. Leukocytes were gated to eliminate consideration of erythrocytes or platelets, and cells staining annexin V-positive/propidium iodide-negative were counted as apoptotic. The results are expressed as the number of apoptotic cells per 100,000 events counted.

Adherent-Cell Analyses. The rats were killed and the implants retrieved on days 7, 14, and 21. Explanted surfaces were washed and adherent cells stained for apoptosis by using annexin V-FITC conjugate (R & D Systems) according to manufacturer instructions. As described elsewhere (3, 4, 11, 12), treated samples were viewed by confocal scanning laser microscopy, and adherent cells staining positive were counted as apoptotic. Apoptotic levels were confirmed for some samples by using the terminal deoxynucleotidyltransferase-mediated dUTP end-labeling method (R & D Systems).

Adherent-cell densities and macrophage fusion were determined after staining by May–Grünwald/Giemsa. Surfaces were rinsed with PBS twice, and adherent cells were fixed by the addition of methanol for 5 min. Cells then were washed with PBS, and May–Grünwald reagent was added for 1 min followed by another PBS wash. Giemsa reagent was added for 5 min followed by a final wash with distilled water. Cell densities were determined from ×5–20 objective fields for each sample and are expressed as cells per mm^2. Nuclei contained within multinucleated FBGCs each were counted as individual cells for determination of cell densities. Percent fusion was calculated by dividing the number of nuclei contained within giant cells by the total number of nuclei in the field of view. This process was repeated for ×3–20 objective fields.

Statistics. The data are expressed as the average of replicate experiments using cells from three different animals ± the standard error of the mean. Statistical comparisons were performed by using the Student's unpaired *t* tests by using STATVIEW 4.1 (Abacus Concepts, Berkeley, CA).

Results

Surface Chemistry-Dependent Induction of Adherent-Cell Apoptosis. Surfaces displaying distinct chemical characteristics were placed in cages and implanted into the dorsum of rats. As shown in Fig. 1 *A*, hydrophilic and anionic surfaces promoted significantly ($P \leq 0.021$) lower rates of adhesion (142 ± 84 and 214 ± 38 cells per mm^2, respectively) when compared with the base surface (746 ± 174 cells per mm^2). In contrast, monocyte adhesion increased on cationic surfaces, reaching significantly increased levels on day 21 (1,551 ± 210 cells per mm^2) when compared with all other surfaces tested.

Adherent cells were stained *in situ* with annexin V-FITC to determine the percentage of adherent cells undergoing apoptosis. As shown in Fig. 1*B*, hydrophilic and anionic surfaces promoted adherent-macrophage apoptosis at increased levels at all time points tested when compared with base surface (polyethylene terephthalate) controls ($P \leq 0.048$ and $P \leq 0.038$, respectively). The largest differences in apoptotic rates were observed on day 14 when hydrophilic surfaces promoted 46 ± 3.7% apoptosis and anionic surfaces 57 ± 5.0% apoptosis, whereas the proportion of apoptotic cells remained relatively low on the base surface (18 ± 1.5%).

Fusion of adherent macrophages was determined by May–Grünwald/Giemsa staining and light microscopy. As shown in Fig. 1*C*, hydrophilic and anionic surfaces provided the lowest levels of macrophage fusion into FBGCs on days 14 and 21 (no fusion observed on hydrophilic surfaces and 4.4–4.6% fusion observed on anionic surfaces), whereas cationic surfaces promoted the highest levels of fusion (80.5 ± 6.7%) on day 21 ($P = 0.03$).

These differences were readily observed qualitatively at day 14 (Fig. 2). The polyethylene terephthalate base surface provides a moderate level of adhesion and fusion (Fig. 2*A*) and a very low percentage of cells staining positive for annexin V-FITC (Fig. 2*B*, note only one brightly stained cell compared with the background fluorescence of the surrounding cells). Hydrophobic surfaces provided a slightly increased level of adhesion and fusion (Fig. 3*C*) when compared with the base surface. Although it appears that the levels of apoptotic cells were increased on these surfaces by the given field of view (Fig. 2*D*), quantitative analyses revealed no statistical significance between the hydrophobic and base surface adherent-cell apoptotic levels (Fig. 1*B*). Adhesion and fusion levels were decreased dramatically on hydrophilic and anionic surfaces (Fig. 2 *E* and *G*), and a large proportion of the adherent cells stained positive for annexin V-FITC (Fig. 2 *F* and *H*, note the relative number of adherent cells on the left to the number of brightly stained cells on the right). Cationic surfaces promoted the highest rate of macrophage fusion (Fig. 2*I*), because the surface was covered almost entirely with FBGCs by this time point (day 14 after implantation).

Effects of Biomaterial Surface Chemistry on Infiltrating Cells. Exudates surrounding the implanted surfaces were collected, inflammatory cells were identified and quantified, and the percentage of apoptotic cells was determined by flow cytometry. As shown in Fig. 3, the percentage of exudate cells surrounding the implants staining positive for apoptosis also was significantly higher for hydrophilic and anionic surfaces at days 7 and 14 ($P \leq 0.003$ and $P \leq 0.01$, respectively). However, these differences in the levels of apoptotic exudate cells around these surfaces were absent by day 21. The percentages of apoptotic cells present in the exudate surrounding all surfaces tested were extremely low, rarely reaching 0.1%.

Total leukocyte counts taken from the exudates surrounding each of the implants revealed that no significant differences were

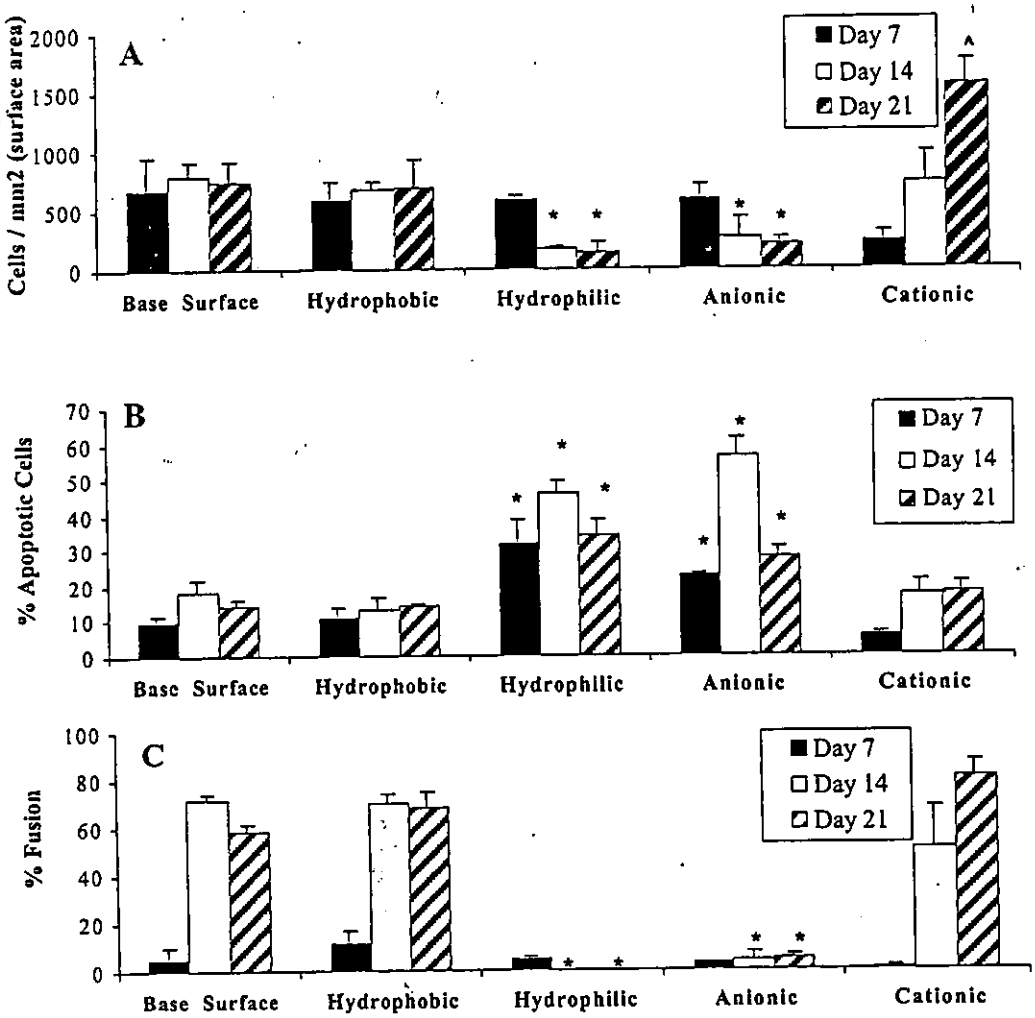

Fig. 1. Adherent-macrophage adhesion, apoptosis, and fusion. Cages were explanted on days 7 (black bars), 14 (white bars), and 21 (hatched bars), surfaces were washed with PBS, and adherent cells were stained with May–Grünwald/Giemsa (*A* and *C*) or annexin V-FITC *in situ* (*B*). (*A*) Cell densities were determined from ×5–20 objective fields for each sample and are expressed as cells per mm^2. (*B*) Samples were viewed by confocal microscopy, and cells staining positive were counted as apoptotic. A total of 200 cells were counted, and the results are expressed as the percentage of the cells that were counted as apoptotic. (*C*) Percent fusion was calculated by dividing the number of nuclei contained within giant cells by the total number of nuclei in the field of view. This process was repeated for ×3–20 objective fields. The data represent mean ± SEM. *, statistical significance, where $P < 0.05$ when compared with the base surface by using the Student's *t* test.

observed in the number of exudate cells between the different chemistries (data not shown). Differential cell counts also displayed no variations in the types or levels of exudate neutrophils, monocytes, or lymphocytes as resolution of the inflammatory response was observed by day 14. Taken together, these data indicate that increased apoptosis is associated with hydrophilic and anionic surfaces, but there is no apparent effect on the surrounding environment, resulting in no prolonged acute or chronic inflammatory reactions.

Discussion

Achieving methods to limit the presence and/or activity of biomaterial-adherent macrophages is essential to promote the functional longevity of implanted medical devices by reducing the cell–material and cell–cell interactions. Adherent-macrophage products such as reactive oxygen species, lysosomal enzymes, and low pH act locally to oxidize and damage the implant surface through mechanisms such as oxidative chain cleavage, hydrolysis, or environmental stress cracking (13, 14). We have shown previously that the fusion of biomaterial-adherent macrophages into FBGCs concentrates these degradative activities to facilitate an increase of surface damage (1, 2). Additionally, adherent monocytes/macrophages/FBGCs play key roles in guiding the response to implanted materials by orchestrating the foreign-body reaction through the production and release of cytokines. The cytokines released by biomaterial-adherent macrophages guide cell–cell interactions by either autocrine or paracrine mechanisms. Chemoattractants such as IL-8 released from adherent macrophages may recruit other leukocytes, namely neutrophils and lymphocytes, to the tissue–material interface. Neutrophils can increase surface damage by generating degradative products through the respiratory burst, whereas lymphocytes interact with adherent macrophages to amplify local cytokine concentrations. The cytokines released by either the lymphocytes (IL-2, IL-4, IL-13, and IL-1β) or adherent macrophages (IL-1β, IL-1RA, TNF-α, and IL-10) further influence the activity of surrounding cells. Additionally, IL-4 or IL-13 produced by these cells induce the fusion of macrophages into FBGCs (15, 16), leading to increased damage of the material as described above. Therefore, methods of reducing these damaging activities by limiting the presence and activity of adherent macrophages are needed to increase the *in vivo* lifetime of

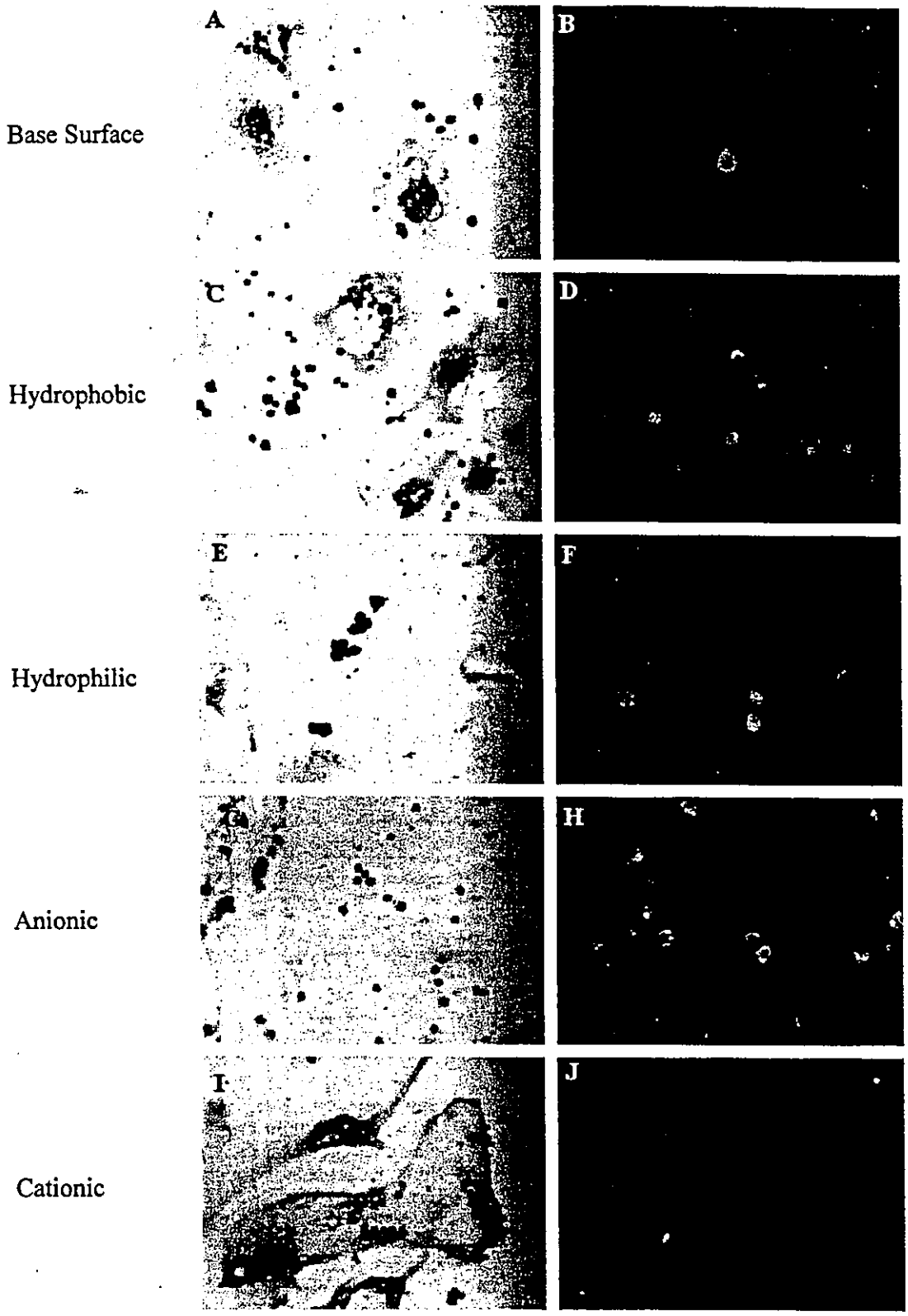

Fig. 2. Morphological properties of macrophages adherent to various surface chemistries. Cages were explanted on day 14, surfaces were washed with PBS, and adherent cells were stained with May–Grünwald/Giemsa and observed by light microscopy (*A*, *C*, *E*, *G*, and *I*) or stained with annexin V-FITC *in situ* and observed by confocal microscopy (*B*, *D*, *F*, *H*, and *J*).

implanted biomaterials, prostheses, and medical devices. Our results from the *in vivo* studies identify apoptosis of biomaterial-adherent monocytes/macrophages as a mechanism for the removal of these cells without generating a prolonged inflammatory response. To this effect, we show that hydrophilic and anionic surfaces promote low levels of adhesion, increased

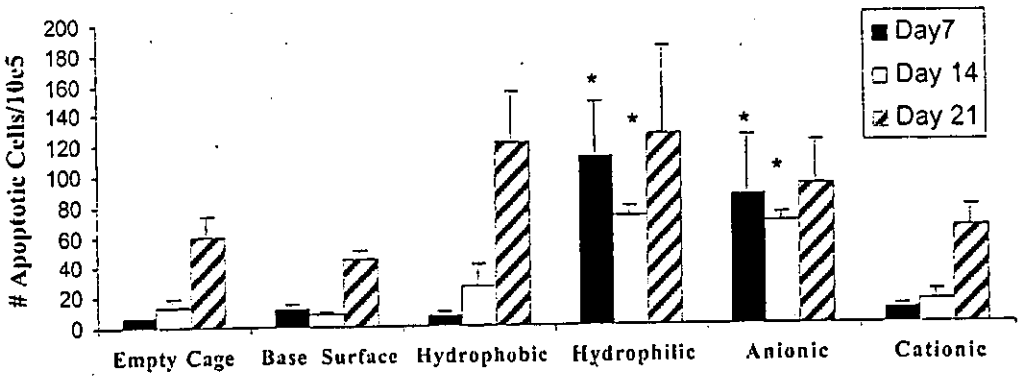

Fig. 3. Exudate cell apoptosis. Exudate surrounding the implant was collected on days 7 (black bars), 14 (white bars), and 21 (hatched bars). One half of the exudate was centrifuged, and cells were stained with annexin V-FITC and propidium iodide. Cells were analyzed immediately by flow cytometry. Leukocytes were gated, and a total of 100,000 events were counted. The data are expressed as the number of cells staining positive out of the total number counted. The data represent mean ± SEM. *, statistical significance, where $P < 0.05$ when compared with the empty cage control using Student's t test.

percentages of apoptosis, and decreased levels of macrophage fusion.

It is likely that differences in adhesion rates result from differences in the adsorbed protein layer that coats the surface of implants immediately after introduction into the body. Previous studies have demonstrated that the types and levels of proteins adsorbed to the implant surface vary among surface chemistries (17, 18). The adsorbed protein layer may include fibrinogen (Fg), fibronectin (Fn), von Willebrand factor (vWF), IgG, and vitronectin (Vn), which act as ligands for protein-specific receptors on the surface of monocytes (19). Therefore, surface chemistry-dependent protein adsorption ultimately may determine the degree of monocyte adhesion. To this extent, decreased rates of monocyte adhesion onto hydrophilic and anionic surfaces may be caused by insufficient numbers or altered conformations of ligands present in the adsorbed protein layer.

The mechanism behind the described surface-dependent apoptosis is not clear; however, as mentioned above the surface-property influence of protein adsorption (17) further modulates the types and levels of cytokines produced (W.G.B., Y.N., T.M., E. Colton, N.P.Z., and J.M.A., unpublished data) because of selective receptor–ligand interactions between the adsorbed protein layer and adherent macrophages. In turn, the levels of cytokines produced by biomaterial-adherent cells locally influence the induction of (by TNF-α or IL-10) or resistance to (by IL-4) apoptosis (12). In accordance with this, we have demonstrated that hydrophilic and anionic surfaces promote increased production of IL-10 (W.G.B., Y.N., T.M., E. Colton, N.P.Z., and J.M.A., unreported observations), a cytokine known to induce apoptosis of adherent cells (20). Additionally, apoptosis is induced by stress caused by geometric constraints (21). Cells adherent to low ligand-containing surfaces (such as the hydrophilic and anionic surfaces) experience low ligand-mediated cell spreading, and maturation is absent, leading to apoptosis by complex signaling mechanisms passed from the nonengaged adhesion receptors to the apoptotic machinery. These two induction mechanisms (increase of IL-10 production and geometric constraints) explain the increased percentage of adherent-macrophage apoptosis observed on hydrophilic and anionic surfaces.

Fusion is a result also of cytokine signaling and protein adsorption. As mentioned above, the wound-healing cytokines IL-4 and IL-13 have been used *in vitro* to promote fusion of adherent macrophages (15, 16). Proximity of adherent cells and appropriate receptor engagements both are needed to promote fusion of adherent macrophages. Once again, hydrophilic and anionic surface chemistries lack the correct adsorbed proteins to promote these mechanisms, whereas cationic surfaces contain abundant ligands to promote adhesion, cell survival, and fusion, which lends support to our previous work linking the parameters of fusion and apoptosis (3), in addition to the fact that no apoptotic FBGCs were observed in any of these studies.

It is of interest to note that the greatest differences in apoptotic levels of cells adherent to the varying surface chemistries were observed on day 14 after implantation. In this respect, it is essential to limit the presence of adherent monocytes/macrophages at early time points to prevent FBGC formation and cytokine release, which would limit long-term structural and chemical damage of the implant by FBGCs and prevent the cytokine-orchestrated formation of an avascular collagenous capsule, providing prolonged implant function.

Although the proportion of adherent cells undergoing apoptosis on hydrophilic and anionic surfaces was increased, relatively few apoptotic cells were observed in the exudate. As time progressed from day 14 to 21, the levels of apoptotic exudate cells increased for all surfaces to the extent where no significant differences were seen among the surfaces. The levels of apoptotic cells observed in the exudate could be accounted for by apoptotic cells released from the surface to the surrounding area, explaining the low levels of apoptotic cells in the exudates, the differences in the levels observed at the earlier time points, and the overall increase over time (because of the accumulation of released cells). These findings also indicate that the mechanism of apoptosis induction is caused by direct interactions between adherent cells and the biomaterial surface and not by released, cell-derived soluble mediators such as cytokines, thereby limiting apoptotic signals to the adherent-cell population. This observation implies a mechanism of induction mediated through the adsorbed protein layer as a function of the surface chemistry. Notably, the induction of apoptosis does not affect the duration or intensity of the inflammatory response as evidenced by the material-independent inflammatory-cell populations in the exudate.

The results presented here agree with previous data regarding implanted prostheses and devices and have implications in their future development. For example, device surfaces used in total hip and knee replacements are hydrophobic and result in eliciting the foreign-body reaction, which is in agreement with expected findings from the data presented here. According to our data, joint prostheses, which use tissue integration into porous surfaces, probably could benefit from surface modifications resulting in hydrophilic and/or anionic properties, because they would reduce the interfacial foreign-body response yet promote bony ingrowth and formation; however, these modifications are not warranted on articular surfaces or with bone cement because of the lack of mechanical

properties. The benefits of hydrophilic surface properties are observed easily with synthetic tendons, where there is no foreign-body reaction to the hydrophilic surface, or cardiovascular and catheter materials, in which reduced blood and tissue interactions are observed with hydrophilic surfaces as opposed to hydrophobic surfaces. Although there is a strong correlation between clinical data and the data presented here regarding surface properties, the role of early surface chemistry-dependent induction of adherent-cell apoptosis in these clinical outcomes is yet to be defined.

Hydrophilic and anionic surface chemistries are the first to be identified to promote increased apoptotic levels of adherent macrophages while limiting adhesion and fusion. This phenomenon represents an ideal mechanism for eliminating the presence of potentially harmful cells from the surface of implanted medical devices and prostheses.

We thank the National Institutes of Health for funding through Grants HL-33849, HL-55714, and GM-20380 (fellowship awarded to W.G.B.).

1. Zhao, Q., Topham, N. S., Anderson, J. M., Hiltner, A., Lodoen, G. & Payet, C. R. (1991) *J. Biomed. Mater. Res.* **25**, 177–183.
2. Ziats, N. P., Miller, K. M. & Anderson, J. M. (1988) *Biomaterials* **9**, 5–13.
3. Brodbeck, W. G., Shive, M. S., Colton, E., Nakayama, Y., Matsuda, T. & Anderson, J. M. (2001) *J. Biomed. Mater. Res.* **55**, 661–668.
4. Shive, M. S., Salloum, M. L. & Anderson, J. M. (2000) *Proc. Natl. Acad. Sci. USA* **97**, 6710–6715.
5. Honma, T. & Hamasaki, T. (1996) *Virchows Arch.* **428**, 165–176.
6. Fabre, T., Belloc, F., Dupuy, B., Schappacher, M., Soum, A., Bertrand-Barat, J., Baquey, C. & Durandeau, A. (1999) *J. Biomed. Mater. Res.* **44**, 429–435.
7. Nakayama, Y. & Matsuda, T. (1996) *Macromolecules* **29**, 8622–8630.
8. DeFife, K. M., Colton, E., Nakayama, Y., Matsuda, T. & Anderson, J. M. (1999) *J. Biomed. Mater. Res.* **45**, 148–154.
9. Marchant, R. E., Hiltner, A., Hamlin, C., Rabinovich, A., Slobodkin, R. & Anderson, J. M. (1983) *J. Biomed. Mater. Res.* **17**, 301–325.
10. Suggs, L. J., Shive, M. S., Garcia, C. A., Anderson, J. M. & Mikos, A. G. (1999) *J. Biomed. Mater. Res.* **46**, 22–32.
11. Shive, M. S., Brodbeck, W. G., Colton, E. & Anderson, J. M. (2001) *J. Biomed. Mater. Res.* **60**, 148–158.
12. Brodbeck, W. G., Shive, M. S., Colton, E. & Anderson, J. M. (2001) *J. Lab. Clin. Med.* **139**, 90–100.
13. Pinchuk, L. (1994) *J. Biomater. Sci. Polym. Ed.* **6**, 225–267.
14. Labow, R. S., Santerre, J. P. & Waghray, G. (1997) *J. Biomater. Sci. Polym. Ed.* **8**, 779–795.
15. McInnis, A. & Rennick, D. M. (1988) *J. Exp. Med.* **167**, 598–611.
16. DeFife, K. M., Jenney, C. R., McNally, A. K. & Anderson, J. M. (1997) *J. Immunol.* **158**, 3385–3390.
17. Jenney, C. & Anderson, J. (2000) *J. Biomed. Mater. Res.* **49**, 435–447.
18. Horbett, T. A. (1993) *Cardiovasc. Pathol.* **2**, 137S–148S.
19. Anderson, J. M., DeFife, K. M., McNally, A. K., Collier, T. O. & Jenney, C. R. (1999) *J. Mater. Sci. Mater. Med.* **10**, 579–688.
20. Wang, Z. Q., Bapat, A. S., Rayanade, R. J., Dagtas, A. S. & Hoffmann, M. K. (2001) *Immunology* **102**, 331–337.
21. Chen, C. S., Mrksich, M., Huang, S., Whitesides, G. M. & Ingber, D. E. I. (1997) *Science* **276**, 1425–1427.

Thermoresponsive Heparin Coating: Heparin Conjugated with Poly(*N*-isopropylacrylamide) at One Terminus

Tomoko Magoshi, Houcin Ziani-Cherif, Shoji Ohya, Yasuhide Nakayama, and Takehisa Matsuda

Department of Bioengineering, National Cardiovascular Center Research Institute, 5-7-1, Fujishiro-dai, Suita, Osaka 565-8565, Japan, and Department of Biomedical Engineering, Graduate School of Medicine, Kyushu University, 3-1-1, Maidashi, Higashi-ku, Fukuoka 812-8582, Japan

Langmuir®
The ACS Journal of Surfaces and Colloids

Reprinted from
Volume 18, Number 12, Pages 4862–4872

Thermoresponsive Heparin Coating: Heparin Conjugated with Poly(*N*-isopropylacrylamide) at One Terminus

Tomoko Magoshi,† Houcin Ziani-Cherif,† Shoji Ohya,† Yasuhide Nakayama,† and Takehisa Matsuda*,‡

Department of Bioengineering, National Cardiovascular Center Research Institute, 5-7-1, Fujishiro-dai, Suita, Osaka 565-8565, Japan, and Department of Biomedical Engineering, Graduate School of Medicine, Kyushu University, 3-1-1, Maidashi, Higashi-ku, Fukuoka 812-8582, Japan

Received September 7, 2001. In Final Form: February 4, 2002

Heparin terminally grafted with a thermoresponsive polymer, poly(*N*-isopropylacrylamide) (PNIPAM), was prepared by sequential steps of chemical modification of one terminal group of heparin, leading to its dithiocarbamylation as an iniferter (*ini*tiator−trans*fer* agent−*ter*minator), followed by quasi-living photopolymerization, thereby producing PNIPAM with a molecular weight (mol wt) ranging from 2×10^3 to 1×10^5 g/mol at the terminus of heparin (PNIPAM−heparin). The lower critical solution temperature depended on the mol wt of PNIPAM. Higher-mol-wt PNIPAM−heparin completely precipitated at 34 °C. The adsorptivity on the poly(ethylene terephthalate) (PET), poly(styrene) (PST), and segmented polyurethane (PU) films was assessed by wettability measurement and surface chemical compositional analysis using X-ray photoelectron spectroscopy. The temperature-dependent amount of adsorbed PNIPAM−heparin was quantitatively determined by a confocal laser scanning microscope (CLSM) using fluorescence-labeled PNIPAM−heparin. The relative degree of heparin complexation with antithrombin III (ATIII) was assessed based on fluorescence intensity using the avidin−biotinylated enzyme complex assay technique under a CSLM. The results showed that irrespective of the type of polymer films, higher-mol-wt PNIPAM−heparin adsorbed better and was more stable than lower-mol-wt PNIPAM−heparin at 40 and 20 °C, an effect which was more enhanced on a hydrophobic surface (PST) than on polar surfaces (PET and PU). The desorption of PNIPAM−heparin did not occur even in the serum-containing medium. In addition, higher complexation capability with ATIII was observed for higher-mol-wt PNIPAM−heparin probably due to its higher adsorption capability. The desorption of PNIPAM−heparin was noted at 20 °C. Thus, it is concluded that PNIPAM−heparin exhibits thermoresponsiveness of surface biofunctionality.

Introduction

Heparin, which is a glycosaminoglycan, has potent anticoagulant activity when complexed with antithrombin III (ATIII) and has been clinically used as an anticoagulant during extracorporeal circulation. Various heparinization techniques applicable to blood-contacting surfaces of extracorporeal devices or catheters have been proposed and developed. These include surface physical mixing,[1,2] coating with the surfactant−heparin complex,[3] surface derivatization through covalent bonding with or without a spacer arm,[4−7] impregnation into a surface hydrogel layer,[11] and complexation onto an animated surface.[8−10]

Physical adsorption is achieved by electrostatically or hydrophobically driven adsorption. In particular, we synthesized a novel "heparin surfactant", in which heparin is terminally derivatized with a long alkyl chain such as lauryl and stearyl groups.[12] Such a heparin surfactant is adsorbed on a polymer surface from an aqueous solution via a hydrophobically driven adsorption process. Physicochemical analyses suggested that the hydrophobic tail of alkylated heparin can anchor on a hydrophobic polymer surface and the heparin molecule is oriented vertically to aqueous media from the surface.

In this study, poly(*N*-isopropylacrylamide) (PNIPAM) with a lower critical solution temperature (LCST) of 32 °C[13] was grafted by polymerization of NIPAM from the dithiocarbamate group, an iniferter (photocleavable radical generator)[14] derivatized on the terminus of heparin. The bioconjugation of heparin and PNIPAM without substantial loss of their bioactivity may be used for adsorption-driven surface modification by simple coating using its aqueous solution at room temperature and concomitant physical stabilization on a substrate surface at a physiological temperature. In this study, we prepared such a thermoresponsive heparin conjugate (PNIPAM−

* To whom correspondence should be addressed. Tel: 81-92-642-6210. Fax: 81-92-642-6212. E-mail: matsuda@med.kyushu-u.ac.jp.

† National Cardiovascular Center Research Institute.

‡ Kyushu University.

(1) Kim, S. W.; Ebert, C. D.; Lin, J. Y.; McRea, J. C. *ASAIO J.* **1983**, *6*, 76−87.

(2) Goosen, M. F. A.; Sefton, M. V. *J. Biomed. Mater. Res.* **1979**, *13*, 347−364.

(3) Leninger, R. I.; Cooper, C. W.; Falb, R. D.; Grode, G. A. *Science* **1966**, *152*, 1625−1626.

(4) Ebert, C. D.; Kim, S. W. *Thromb. Res.* **1982**, *26*, 43−57.

(5) Yuan, S.; Cai, W.; Szakalas-Gratz, G.; Kottke-Marchant, K.; Tweden, K.; Marchant, R. E. *J. Appl. Biomater.* **1995**, *6*, 259−266.

(6) Larm, O.; Larsson, R.; Olsson, P. A. *Biomater., Med. Devices, Artif. Organs* **1983**, *11* (2−3), 161−173.

(7) Olsson, P.; Sanchez, J.; Mollnes, T. E.; Riesenfeld, J. *J. Biomater. Sci., Polym. Ed.* **2000**, *11*, 1261−1273.

(8) Holland, F. F.; Gidden, H. E.; Mason, R. G.; Klein, E. *Artif. Organs* **1978**, *1*, 24−36.

(9) Barbucci, R.; Baszkin, A.; Benvenuti, M.; de Lourdes Costa, M.; Ferruti, P. *J. Biomed. Mater. Res.* **1987**, *21*, 443−457.

(10) Tanzawa, H.; Mori, Y.; Harumiya, N.; Miyama, H.; Hori, M.; Oshimu, N.; Idezuki, Y. *Trans.−Am. Soc. Artif. Intern. Organs* **1973**, *19*, 188−194.

(11) Goosen, M. F. A.; Sefton, M. V. *J. Biomed. Mater. Res.* **1983**, *17*, 359−373.

(12) Matsuda, T.; Magoshi, T. *Biomacromolecules* **2001**, *2*, 1169−1177.

(13) Heskins, M.; Guillet, J. E. *J. Macromol. Sci., Chem.* **1968**, *A2*, 1441−1455.

(14) Otsu, T.; Matsumoto, A. *Adv. Polym. Sci.* **1998**, *136*, 75.

10.1021/la011408s CCC: $22.00
Published on Web 05/17/2002

heparin). Its complexation with ATIII was assessed with a confocal laser scanning microscope using an antibody–enzyme-based chromogenic substrate. In this paper, the preparation of PNIPAM-grafted heparin was described, followed by graft chain length dependency of its surface adsorption/desorption and biological activity characteristics.

Experiments

Reagents. 4-(Chloromethyl)benzoic acid and NIPAM were purchased from Tokyo Kasei Co. (Tokyo, Japan). ATIII and bovine serum albumin (BSA) were obtained from Sigma Chemicals Co. (St. Louis, MO). Other reagents and solvents were obtained from Wako Pure Chemicals Inc. (Osaka, Japan). The poly(ethylene terephthalate) (PET), poly(styrene) (PST), and segmented polyurethane (PU) films were obtained from Bellco Glass Inc. (Vineland, NJ), Minamide Corp. (Osaka, Japan), and Nihon Zeon Co. (Tokyo, Japan), respectively. All solvents and reagents were of special grade and used without further purification, except for NIPAM which was recrystallized from toluene–hexane and stored in the refrigerator.

General Methods. Purification of heparin, oxidized heparin, and PNIPAM–heparin was carried out using a dialysis membrane (molecular weight (mol wt) cutoff level = 12 000–14 000, Wako). The ion-exchange was performed using a Dowex 50 × 8 (H^+) resin (Dow Chemicals, Midland, MI). ^{1}H NMR spectra were recorded in $CDCl_3$ using tetramethylsilane as the internal standard with a JNM-GX270 FT-NMR spectrometer (JEOL, 270 MHz, Tokyo, Japan). UV/vis spectra were recorded using a Ubest-30 UV/vis spectrophotometer (Japan Spectroscopic Co., Ltd., Tokyo, Japan). X-ray photoelectron spectroscopy (XPS) was performed to determine the surface chemical composition using an ESCA-3400 instrument (Shimadzu Corp., Kyoto, Japan) at the takeoff angle of 90°. Wettability of the treated surfaces was evaluated using the sessile drop technique with a contact angle meter (CA-D, Kyowa Interface Science Co., Ltd., Saitama, Japan). The fluorescence image of the surface was observed using a confocal laser scanning microscope (MRC-1024, 543 nm exDitation; Bio-Rad Lab., Hercules, CA).

Synthesis of Lactone-Terminated Heparin [2]. The detailed preparation is according to the method described by Sugiura et al.[15] Heparin sodium salt (4.0 g, mol wt = 1.2 × 10^4; 198.6 IU/mg) was dissolved in deionized water and passed through a Dowex 50 × 8 (H^+) column. The eluate was dialyzed and then lyophilized to yield heparin (3.8 g, 0.32 mmol). The reducing end of heparin was oxidized with iodide (0.8 g, mmol) in 20% aqueous methanol solution (100 mL) for 6 h at room temperature. The reaction solution was added to ethanol containing 4% potassium hydroxide (200 mL). The white precipitate was obtained by filtration and dissolved in deionized water, and the resulting solution was dialyzed. Upon freeze-drying of the dialyzed solution, oxidized heparin was obtained. The oxidized heparin was dissolved in deionized water and passed through a Dowex 50 × 8 (H^+) column. Upon freeze-drying of the eluate, lactone-terminated heparin [2] was obtained (3.0 g; yield, 78%).

4-(*N,N*-Diethyldithiocarbamoylmethyl)benzoic Acid [4]. Sodium *N,N*-diethyldithiocarbamate trihydrate (10.6 g, 46.9 mmol) and sodium iodide (4.4 mg, 2.9 mmol) were added to an ethanolic solution (150 mL) of 4-(chloromethyl)benzoic acid [3] (5.0 g, 29.3 mmol). The mixture was refluxed for 4 h and then stirred overnight at room temperature. After evaporation of ethanol, the crude mixture was neutralized with 10% cold aqueous hydrochloric acid solution and the product was extracted with ethyl acetate three times. The organic layer was dried using sodium sulfate, filtered with a pad of Celite, and evaporated under reduced pressure. The product of purification was confirmed by thin-layer chromatography (TLC). The results were as follows. Yield: 8.3 g, 99%. TLC: R_f = 0.7 ($CHCl_3/CH_3OH$ = 80/20). ^{1}H NMR ($CDCl_3$, δ ppm): 8.04 (*d*, 2H, Ar-*H*), 7.48 (*d*, 2H, Ar-*H*), 4.63 (s, 2H, Ar–CH_2), 4.05 (*m*, 2H, CH_2N), 3.75 (*m*, 2H, CH_2N), and 1.29 (*t*, 6H, CH_3).

4-[(*N,N*-Diethyldithiocarbamoylmethyl)-2-aminoethyl]benzamide [6]. Oxalyl chloride (5.0 mL, 58.2 mmol) and two drops of *N,N*-dimethylformamide (DMF) were added to a solution of acid **4** (6.6 g, 23.3 mmol). The mixture was stirred at room temperature for 3 h and then concentrated under reduced pressure. Addition of toluene (50 mL) followed by evaporation of the solution under reduced pressure was repeated twice to remove excess oxalyl chloride. Crude acid chloride [5] was then dissolved in methylene chloride (200 mL) and cooled to 0 °C in an ice bath. A solution of ethylenediamine (16 mL, 233 mmol) in methylene chloride solution (50 mL) was added dropwise with vigorous stirring at 0 °C, and the reaction mixture was stirred overnight at room temperature. The solvent was evaporated under reduced pressure, and the product was purified by silica gel column chromatography (elution: $CHCl_3/CH_3OH$ = 90/10 with ($CH_3CH_2)_3$N (1%)). The results were as follows. Yield: 6.7 g, 88%. TLC: R_f = 0.15 ($CHCl_3/CH_3OH$ = 80/20). ^{1}H NMR ($CDCl_3$, δ ppm): 7.74 (*d*, 2H, Ar-*H*), 7.43 (*d*, 2H, Ar-*H*), 6.83 (*s*, 1H, N*H*), 4.59 (*s*, 2H, CH_2S), 4.04 (*m*, 2H, CH_2N), 3.70 (*m*, 2H, CH_2N), 3.49 (*m*, 2H, CH_2N), 2.94 (*m*, 2H, CH_2N), 1.99 (*s*, 2H, NH_2), and 1.28 (*t*, 6H, CH_3).

Heparin Derivatized with Dithiocarbamate Iniferter [7]. Compound **6** (162 mg, 5.0 × 10^{-4} mol) in DMF (5.0 mL) was added to lactone-terminated heparin (300 mg, 0.025 mmol) solution in DMF (17 mL) and then neutralized with tri-*n*-butylamine (0.1 mL). The mixture was stirred for 16 h at 80 °C under an argon atmosphere. After evaporation of the solvent under vacuum, the residue was dissolved in deionized water (20 mL) and the solution was passed through a Dowex 50 × 8 (H^+) column. Upon freeze-drying of the eluate, the product was then freeze-dried to yield a pale brown solid **7** (270 mg, 90%).

Polymerization of NIPAM Initiated with Compound [7]. Photopolymerization initiated using compound **7** was performed in an aqueous solution of NIPAM under a nitrogen atmosphere with UV irradiation (light intensity, 0.5 mW/cm^2) using a 250 W Hg lamp (SPOT CURE, USHIO, Tokyo, Japan). After polymerization, the reaction mixture was dialyzed followed by freeze-drying to yield a white or pale brown solid (PNIPAM–heparin [8]).

Fluorescence-Labeled PNIPAM–Heparin. Fluorescence-labeled PNIPAM–heparins were prepared by condensation reaction with 5-(4,6-dichlorotriazin-2-yl)aminofluorescein (DTAF, Sigma) according to our method previously reported[12] (the number of fluorescent dye molecules conjugated to heparin ranged from 2 to 5 per molecule).

Transmittance Measurement. The LCST of PNIPAM–heparin was determined by measuring the optical transmittance at 600 nm of an aqueous PNIPAM–heparin solution (0.5 wt %) at a heating rate of 0.5 °C/min from 25 to 40 °C. The temperature at onset of decrease in transmittance, which was determined with an accuracy of 0.1 °C by a thermosensor that was directly immersed into a solution, was defined as the LCST.

Adsorption and Desorption. The PNIPAM–heparin-coated PET film was prepared as follows. An aqueous solution of PNIPAM–heparin [8] (0.5 wt %, 5 μL) was placed on the surface of a circular PET film (diameter, 15 mm), and the film was dried at 20 °C. The film surface was rinsed with either cold water (20 °C) or hot water (40 °C). Alternatively, PNIPAM–heparin-adsorbed PET film was prepared by immersion in a 0.5 wt % aqueous solution of PNIPAM–heparin [8] (PNIPAM mol wt = 1 × 10^4) at 20 °C. Then, the film was immersed in a solution at either 20 or 40 °C for 3 h. Then, the film surface was rinsed with either cold water (20 °C) or hot water (40 °C).

Adsorbed PNIPAM–Heparin. The amounts of adsorbed PNIPAM–heparin on surfaces were determined by measurement of average fluorescence intensity of fluorescence-labeled PNIPAM–heparin-coated surfaces under a confocal laser scanning microscope (CLSM) using the standard linear relationships between the fluorescence intensity and the amount of fluorescence-labeled PNIPAM–heparins.

Antithrombin III Trapping. The PNIPAM–heparin-treated film surface was treated with 1% BSA in phosphate-buffered solution (PBS) for 30 min to block nonspecific adsorption of ATIII or antibodies and then immersed in the ATIII-containing PBS (1 unit/mL) for 30 min at 4 °C. Then, the films were thoroughly washed with a buffer solution for fluorescence staining. The

(15) Sugiura, N.; Sakurai, K.; Karasawa, K.; Sakurai, S.; Kimata, K. *J. Biol. Chem.* **1993**, *268*, 15779–15787.

Scheme 1. Reactions for Synthesis of PNIPAM–Heparin

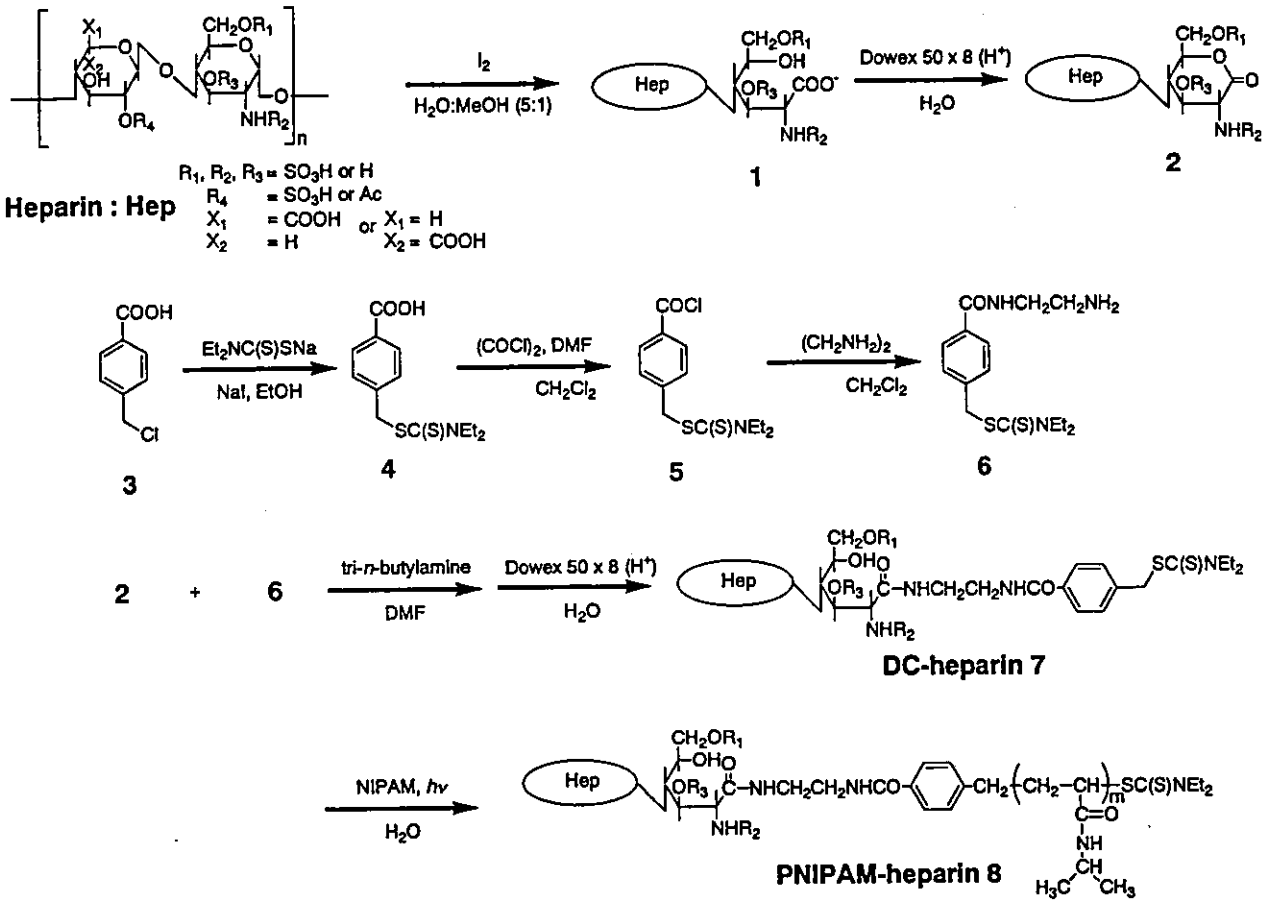

PNIPAM–heparin–ATIII complex coated film surfaces were treated by an enzyme-labeled-antibody technique using an ABC kit (Vector Laboratories, Inc., Burlingame, CA) and visualized under the CLSM. The treated films were incubated in the medium DMEM (Dulkecco's modified Eagle's medium; Gibco, Grand Island, NY) containing 10% fetal bovine serum (FBS, Life Technologies, USA) to see whether PNIPAM–heparin is stably anchored on the surface in a body-simulated fluid. Staining was performed according to the manufacturer's instruction. Briefly, the first step involves treatment with a buffer solution containing a sheep monoclonal antibody. Then, a buffer solution containing a biotinylated secondary antibody was applied; an avidin solution and a biotinylated alkaline phosphatase (AP) solution were subsequently applied to the film surface. An AP substrate was used for chromogenic staining. The colorimetric enzyme–substrate reaction allows visualization of fixed proteins only. The film surfaces were imaged using the CLSM. The ABC–AP substrate conjugated maximum excitation closely matches the 543-nm spectral line of the argon-ion laser, making it the fluorochrome of choice for the CLSM.

Results

Preparation of PNIPAM-Grafted Heparin [8]. Heparin, terminally grafted with PNIPAM, was prepared by sequential reactions involving oxidation cleavage (compound **1**, Scheme 1), lactone ring formation (compound **2**), and dithiocarbamylation (compound **7**) at the terminal sugar moiety and subsequent photopolymerization, which was initiated from the dithiocarbamate (DC) group at the terminus of heparin, producing PNIPAM-grafted heparin (PNIPAM–heparin; compound **8**). The former two steps were carried out following a previously reported method using iodine-induced cleavage and subsequent proton-catalyzed cyclization.[15] This method has been proven to cause minimal damage to both backbone and side chains of polysaccharides.[15] Dithiocarbamylation was conducted by a ring-opening reaction of lactone-terminated heparin [2] with DC-derivatized ethylenediamine (compound **6**), which was prepared using 4-chloromethyl benzoic acid (compound **3**) as a starting material. UV irradiation of an aqueous solution containing DC-derivatized heparin [7] in the presence of NIPAM resulted in successive photopolymerization initiated from the terminus of the heparin molecule in a living polymerization fashion, which was deduced from previous papers.[16,17]

To estimate the molecular weight of the PNIPAM graft chain, we utilized our recently reported reaction condition–molecular weight relationship, which was established using the iniferter poly(ethylene glycol) having a DC group at one end and a methyl group at the other end (DC–PEG).[21] In the present experiments, the reaction condition (photointensity, 0.5 m W/cm^2; photoirradiation time, 30 min) was the same as that previously reported. On the basis of this reaction condition–molecular weight relationship, we assumed that the estimated number-average molecular weights of the PNIPAM graft chains of heparin, thus prepared, ranged from approximately 2×10^3 to 1×10^5 g/mol and the polydispersity index was approximately 1.2–1.3, which depends on the DC and NIPAM concentrations (Table 1). An increase in NIPAM concentration and a decrease in the DC–heparin concentration resulted in higher-mol-wt PNIPAM grafted at the terminal end of heparin.

The resultant PNIPAM–heparin [8] was a white solid and dissolved in water at room temperature but precipi-

(16) Nakayama, Y.; Matsuda, T. *Macromolecules* **1999**, *32*, 5405.
(17) Lee, H. J.; Nakayama, Y.; Matsuda, T. *Macromolecules* **1999**, *32*, 6989.

Table 1. Estimated Mol Wt of PNIPAM–Heparin Prepared at Different Molar Concentrations of Iniferter and Monomer and Thermoresponsive Properties

sample	DC–heparin[a] [mmol/L]	NIPAM [mmol/L]	mol wt of PNIPAM chain[b] (× 10^4 g/mol)	LCST[c] (°C)	equilibrium transmittance (%)
a	0.50	10	0.2	37.1 ± 0.4	49
b	0.50	10	0.5	35.1 ± 0.3	85
c	0.01	10	1.0	34.6 ± 0.1	100
d	0.01	50	5.0	34.0 ± 0.1	100
e	0.01	100	10.0	34.0 ± 0.1	100

[a] Iniferter-derivatized dithiocarbamyl heparin (compound 7 in Scheme 1). [b] Estimated from polymerization behavior using dithiocarbamyl poly(ethylene glycol), DC–PEG, under the same conditions described in our previous paper. [c] Lower critical solution temperature at 0.5% concentration.

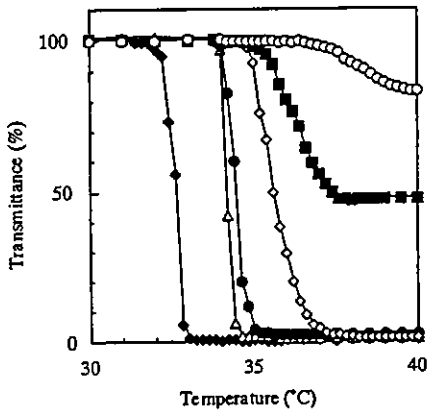

Figure 1. Thermoresponsive change in transmittance of PNIPAM–heparin with PNIPAM of different mol wt's in aqueous solution. The mol wt of PNIPAM in PNIPAM–heparin: 2 × 10^3 (○), 5 × 10^4 (■), 1 × 10^4 (◇), 5 × 10^4 (●), and 1 × 10^5 (△); PNIPAM homopolymer (◆). Concentration of PNIPAM–heparin: 1 wt %. Heating rate: 0.5 °C/min.

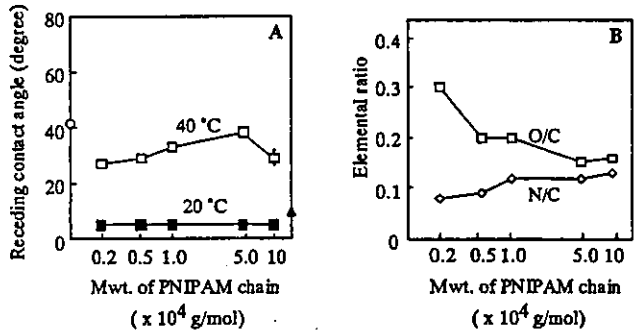

Figure 2. (A) Receding contact angles of PNIPAM–heparin-coated surfaces washed with water at 20 °C (□) or 40 °C (■). (A) Nontreated PET film (○) and PNIPAM homopolymer (▲). (B) Elemental ratios measured by XPS of the PNIPAM–heparin-coated surface: O/C (□) and N/C (●). The film surfaces were washed with water at 40 °C. Theoretical elemental ratios of sodium heparin salt were as follows: O/C, 0.65; N/C, 0.04; S/C, 0.12. Theoretical values of PNIPAM homopolymer were as follows: O/C, 0.17; N/C, 0.17.

tated in the physiological temperature range. Figure 1 shows the thermoresponsive change in transmittance of PNIPAM–heparin in 1% aqueous solution. The PNIPAM homopolymer (mol wt = 2 × 10^5 g/mol), which was prepared by radical polymerization in a previous study, exhibited a very sharp drop in transmittance at approximately 31.9 ± 0.1 °C and completely precipitated above this temperature. Table 1 also lists the LCST of PNIPAM–heparins with different mol wt graft chains. For PNIPAM–heparins with higher-mol-wt PNIPAM (PNIPAM mol wt = 5 × 10^4 and 1 × 10^5 g/mol), a sharp drop in transmittance and LCST of approximately 34.0 ± 0.1 °C were noted. For PNIPAM–heparins with lower-mol-wt PNIPAM, a gradual increase in LCST, a temperature-dependent drop in transmittance, and a high equilibrium transmittance were noted. LCST is gradually increased as the molecular weight of the PNIPAM graft chain is decreased. For example, PNIPAM–heparin with the PNIPAM mol wt of 1 × 10^4 g/mol exhibited complete precipitation at 34.6 ± 0.1 °C, whereas PNIPAM–heparin with a lower-mol-wt PNIPAM exhibited incomplete precipitation (equilibrium transmittance and LCST were approximately 85% and 35.1 ± 0.3 °C, respectively, for PNIPAM with the mol wt of 5 × 10^3 g/mol and approximately 49% and 37.1 ± 0.4 °C for that with the mol wt of 2 × 10^3 g/mol, respectively).

Thermoresponsive Adsorption/Desorption Characteristics on PET. The PET samples were coated with a 0.5 wt % aqueous solution of PNIPAM–heparin [8] and subsequently air-dried and subjected to washing with water at either 20 or 40 °C. The mol wt dependency for PNIPAM–heparin [8] of wettability and surface composition is shown in Figure 2. Irrespective of the mol wt of PNIPAM, the receding contact angle for samples washed with water at 40 °C was less than 10°, which is almost the same as that of the PNIPAM homopolymer (12°) (Figure 2A). On the other hand, the receding contact angle for samples washed with water at 20 °C was quite high, 30–40°, which is lower than that of the homopolymer (49.2°) but close to that of the noncoated PET film. XPS measurement (determined at the takeoff angle of 90 °C) of samples washed with water at 40 °C showed that an increase in the mol wt of PNIPAM increased N/C and decreased O/C, both of which approached the theoretical values of the PNIPAM homopolymer (0.17 for each) (Figure 2B). Figure 3 shows high-resolution C_{1S} and O_{1S} XPS spectra obtained for PNIPAM–heparin with the highest mol wt graft chain (1 × 10^5 g/mol) (Figure 3B). Upon washing at 40 °C, subpopulations of C_{1S} and O_{1S} were quite apart from those of the nontreated PET films: for the C_{1S} subpopulation, the carbonyl carbon peak at 289.0 eV relative to the C–N or C–O peak at 286.7 eV (note that hydrocarbon carbon is standardized at 285.0 eV) became larger, and for the O_{1S} subpopulation, the carbonyl oxygen peak (532.7 eV) relative to the ether or hydroxy oxygen peak (534.3 eV) also became larger, whereas upon washing at 20 °C, these relative peak intensities tended to decrease but were still larger than that of nontreated PET film. Since the carbonyl group is mainly derived from the PNIPAM molecule, these results strongly indicate that PNIPAM–heparin with a high mol wt graft chain covered the outermost surface of the adsorbed layer on PET at 40 °C, but some fraction of adsorbed PNIPAM–heparin apparently desorbed upon washing at 20 °C. This temperature dependence of adsorption/desorption was more markedly observed for PNIPAM–heparin with the lowest mol wt of PNIPAM. From C_{1S} and O_{1S} spectral analysis, a low extent of adsorption at 40 °C and a high extent of desorption at 20 °C were clearly noticed (Figure 3A).

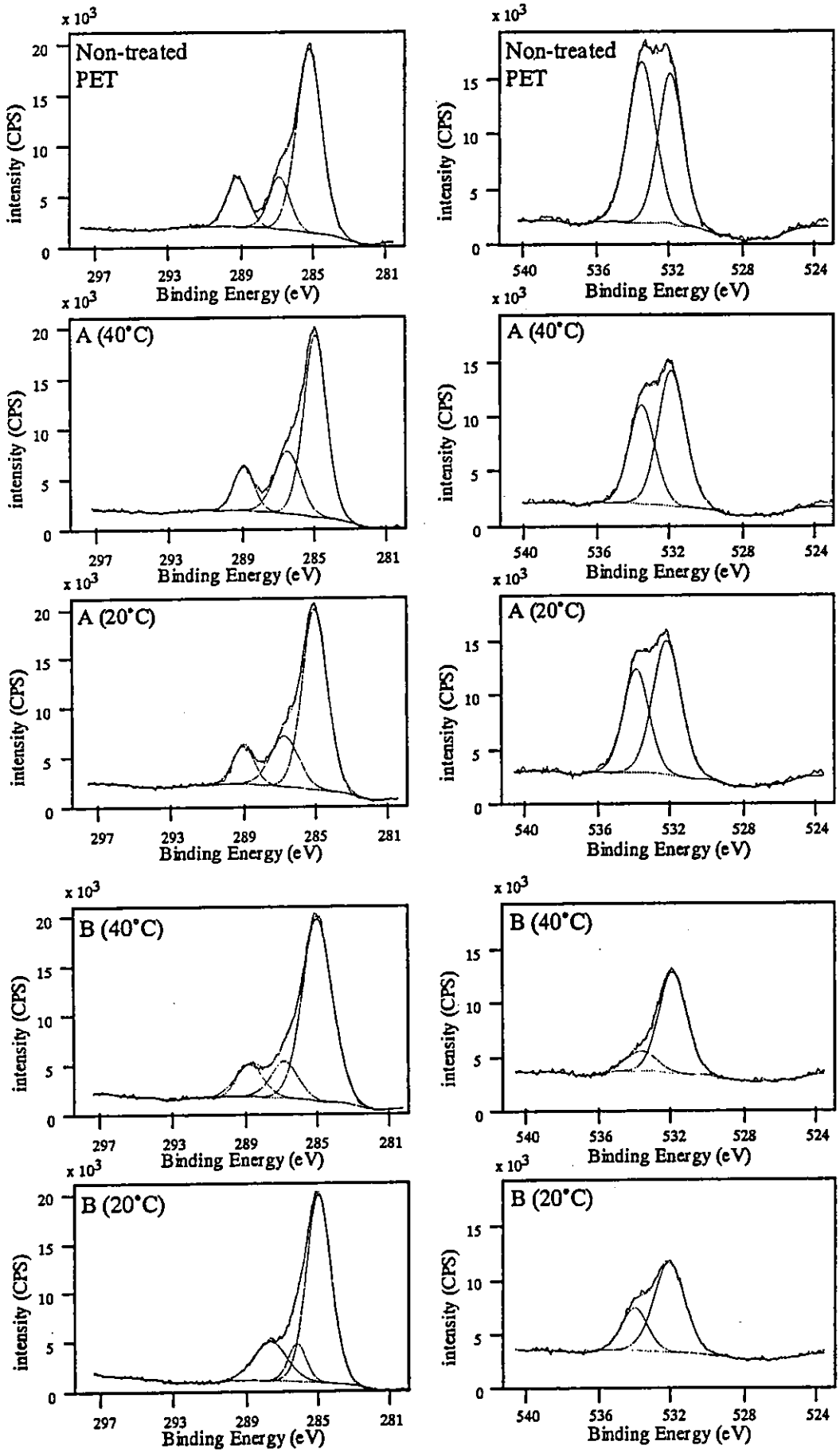

Figure 3. High-resolution C_{1S} and O_{1S} spectra of PNIPAM–heparin-adsorbed and -desorbed PET surfaces: (A) nontreated PET and (B) treated with PNIPAM–heparin with a graft chain mol wt of 2×10^3 g/mol.

Table 2. Temperature Dependence of Wettability and Surface Chemical Composition at Adsorption and Washing Steps on the PET Surface[a]

sample	temperature (°C)		water contact angle (deg)		elemental ratio	
	adsorption	washing	advancing	receding	O/C	N/C
nontreated PET			59.0 ± 1.8	41.8 ± 1.9	0.34 (0.40)	
c1	20	20	65.8 ± 4.0	33.5 ± 2.9	0.22	0.06
c2	40	20	64.5 ± 4.5	32.7 ± 1.6	0.20	0.09
c3	40	40	52.5 ± 11.5	13.7 ± 5.3	0.17	0.10
PNIPAM	40	40	49.2 ± 10.0	10.8 ± 1.5	0.12 (0.17)	0.15 (0.17)

[a] PNIPAM–heparin with a PNIPAM graft chain mol wt of 1×10^5 g/mol was used.

Table 3. Amount of Adsorbed PNIPAM–Heparin before and after Washing at 40 and 20 °C ($n = 3$)

fluorescence-labeled PNIPAM–heparin (mol wt of PNIPAM chain, g/mol)	amount of coating (μg/mm^2)	remaining PNIPAM–heparin (μg/mm^2) after washing		percent of remaining amount after washing (%)	
		20 °C	40 °C	20 °C	40 °C
2×10^3	2.40 ± 0.15	0.87 ± 0.06	1.28 ± 0.03	36.4	53.4
1×10^4	2.62 ± 0.08	1.11 ± 0.01	1.61 ± 0.03	42.8	61.8
1×10^5	2.60 ± 0.30	2.00 ± 0.06	2.36 ± 0.20	76.4	90.1

Table 4. Temperature Dependence of Wettability and Surface Chemical Composition at Adsorption and Washing Steps on PST and PU Surfaces[a]

material	mol wt of PNIPAM chain($\times 10^4$ g/mol)	water contact angle (deg) (washing temperature)				elemental ratio (washing temperature)			
		20 °C		40 °C		20 °C		40 °C	
		advancing	receding	advancing	receding	N/C	O/C	N/C	O/C
PS	nontreated	85.9 ± 1.2	85.5 ± 1.4	79.5 ± 0.8	81.1 ± 1.3	0.00	0.01		
	0.2	67.7 ± 1.6	30.0 ± 1.1	64.2 ± 2.9	32.6 ± 10.7	0.03	0.07	0.02	0.04
	1.0	63.3 ± 0.4	37.2 ± 1.6	66.1 ± 3.6	20.4 ± 10.7	0.05	0.10	0.08	0.12
	10.0	39.0 ± 5.4	15.9 ± 9.5	46.0 ± 12.8	12.5 ± 1.8	0.10	0.14	0.11	0.14
PU	nontreated	73.0 ± 1.6	49.7 ± 0.7	73.4 ± 1.7	44.9 ± 1.7	0.03	0.26		
	0.2	68.3 ± 2.4	45.1 ± 1.4	70.3 ± 2.3	42.9 ± 1.6	0.03	0.33	0.03	0.27
	1.0	76.1 ± 4.1	45.7 ± 1.8	26.5 ± 4.1	<10	0.04	0.26	0.13	0.18
	10.0	72.7 ± 3.5	41.0 ± 4.1	22.3 ± 9.6	<10	0.04	0.25	0.11	0.20

[a] PNIPAM–heparin samples with different mol wt graft chains were used.

The amounts of adsorbed PNIPAM–heparin, which were determined using fluorescence-labeled PNIPAM–heparin in which the hydroxyl group was partially derivatized with a fluorescent dye (DTAF) according to our method previously reported[12] using the CSLM, were as follows: A fixed amount (2.60 μg/nm^2) of PNIPAM–heparin with a PNIPAM mol wt of 2×10^3 and 1×10^5 was coated on PET films. After being air-dried, the films were subjected to immersion into water at 20 or 40 °C for 6 h, and subsequently the surface fluorescence was scanned under the CLSM. Table 3 lists the remaining amount of PNIPAM–heparin with different mol wt graft chains, which was calculated from the predetermined standard linear relations between the amount of fluorescence-labeled PNIPAM–heparin and fluorescence intensity. At 40 °C, a larger amount of remaining PNIPAM–heparin was observed for PNIPAM–heparin with the highest mol wt (2×10^3), followed by PNIPAM–heparin with an intermediate mol wt of PNIPAM (1×10^4). The lowest adsorption amount at 40 °C and highest desorption amount was found for PNIPAM–gelatin with a lower mol wt (2×10^3). Table 3 also lists the percentage of remaining amount of PNIPAM–heparin upon washing at 40 or 20 °C: a higher mol wt of PNIPAM leads to higher adsorption at 40 °C and low desorption at 20 °C. A lower mol wt of PNIPAM–heparin apparently desorbed considerably at 20 °C.

Substrate Dependency on Adsorptivity/Desorptivity. It is of interest to know whether such thermoresponsiveness of adsorption and desorption depends on the type of substrate films. To this end, substrate dependency of thermoresponsiveness of adsorption and desorption of PNIPAM–heparin was carried out as follows. In addition to PET as mentioned above, two polymeric films (PST and PU) were studied. Table 4 lists surface chemical compositions (determined by XPS) and wettabilities (determined by advancing and receding contact angles). Irrespective of the type of polymer films, the general tendency is as follows: (1) An increase in the mol wt of the PNIPAM chain appears to increase the N/C ratio but to reduce the O/C ratio, irrespective of temperature. A marked increase in the N/C ratio was observed for the highest mol wt of PNIPAM. (2) In general, the N/C ratio at 40 °C was higher than that at 20 °C. Since the nitrogen atom is mainly derived from the PNIPAM molecule, an increase in the N/C ratio means that PNIPAM–heparin adsorbs well on the polymer surface at 40 °C. High-resolution C_{1s} spectra of samples before and after coating/washing provide more detailed information on adsorption and desorption characteristics, as shown in Figures 4 and 5. For PST, with an increase in the mol wt of the graft chain, the relative intensity fraction of carbonyl carbon in the C_{1s} spectra of both PST and PU films, both of which were subjected to washing at 40 °C, was increased. However, upon washing at 20 °C, a considerably large fraction of carbonyl carbon disappeared in the spectra of both films, irrespective of the mol wt of the graft chain, except for PST coated with PNIPAM–heparin with the highest mol wt graft chain; there is little difference in the fine structure of the C_{1s} spectra and wettability between 20 and 40 °C (Table 4). From XPS and wettability measurements, it can be said that the desorption was easier for PET and PU as compared with PST.

Complexation with ATIII. It is of primary importance to determine whether PNIPAM–heparin adsorbed on surfaces can be complexed with ATIII since the antithrombin activity of ATIII is markedly increased by complexation with heparin. After the PET films were

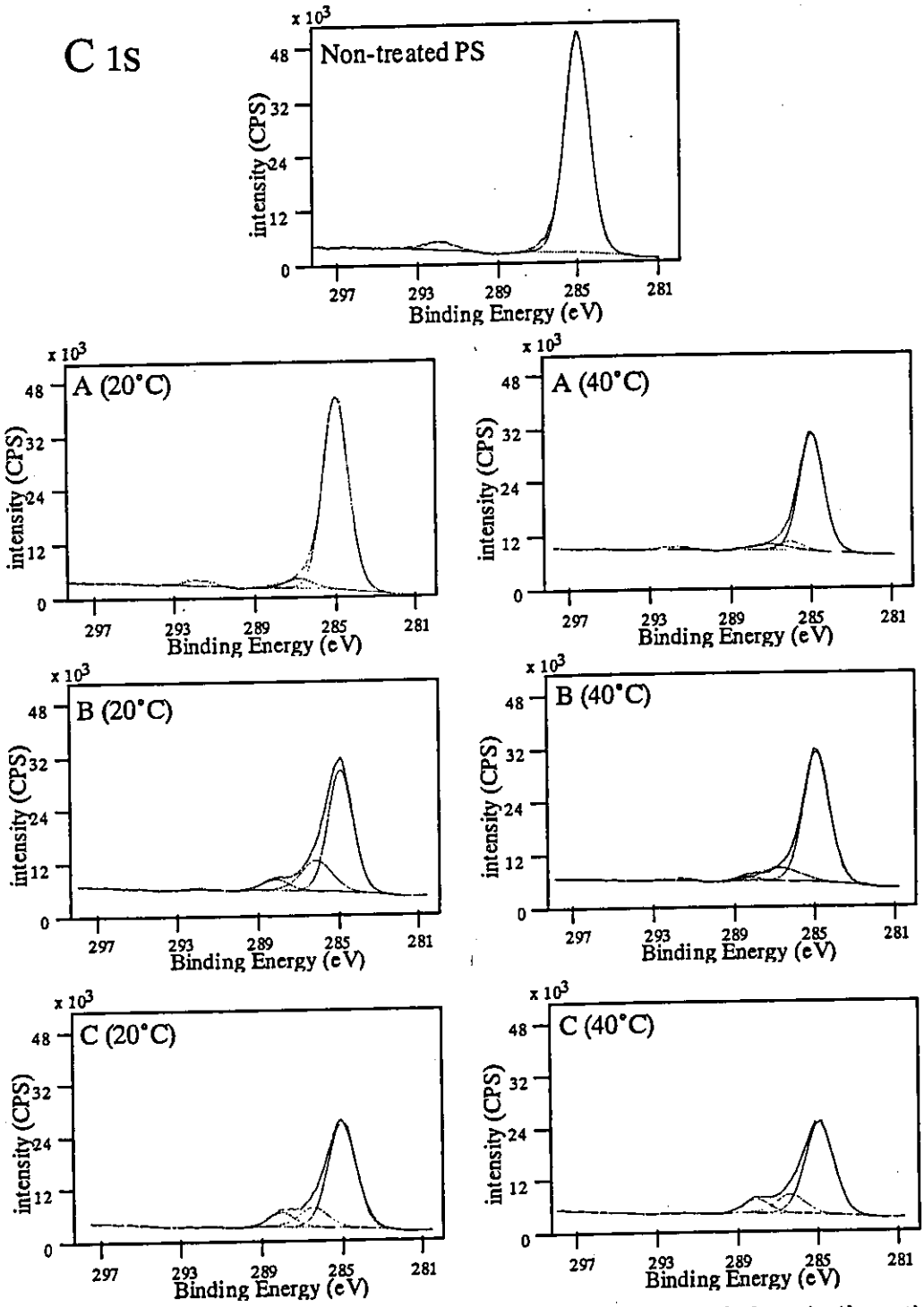

Figure 4. High-resolution C_{1s} spectra of polystyrene films with or without treatments of adsorption/desorption of PNIPAM–heparin with different mol wt graft chains. The mol wt of graft chains: (A) 2×10^3 g/mol, (B) 1×10^4 g/mol, and (C) 1×10^5 g/mol. Temperature denotes the washing temperature.

immersed in a 1% aqueous solution containing PNIPAM–heparin and dried, the films were washed with water at 40 °C. Subsequently, the films were immersed in an albumin-containing buffer solution for 1 h and immersed in an ATIII-containing buffer solution according to the instructions on the use of the ABC (avidin–biotinylated enzyme complex) kit; immunostaining was carried out by sequential treatment using an anti-ATIII antibody, biotinylated IgG, and avidin-coupled alkaline phosphatase and final staining using a chromogenic substrate. All of these steps were carried out at 40 °C. Figure 6A shows the fluorescence intensity dependence on the mol wt of PNIPAM, which was determined using the CLSM. Figure 6B strongly indicates that the relative fluorescence intensity (nontreated PET film was used as a control) increased significantly with an increase in the mol wt of the PNIPAM chain, indicating that high-mol-wt PNIPAM–heparin has a much greater capacity for complexation with ATIII than low-mol-wt PNIPAM–heparin.

Temperature-Dependent Adsorption/Desorption and Complexation with ATIII. The temperature dependency of coating and washing steps upon adsorption and desorption of PNIPAM–heparin and its ATIII complexation was determined as follows. The PET films were

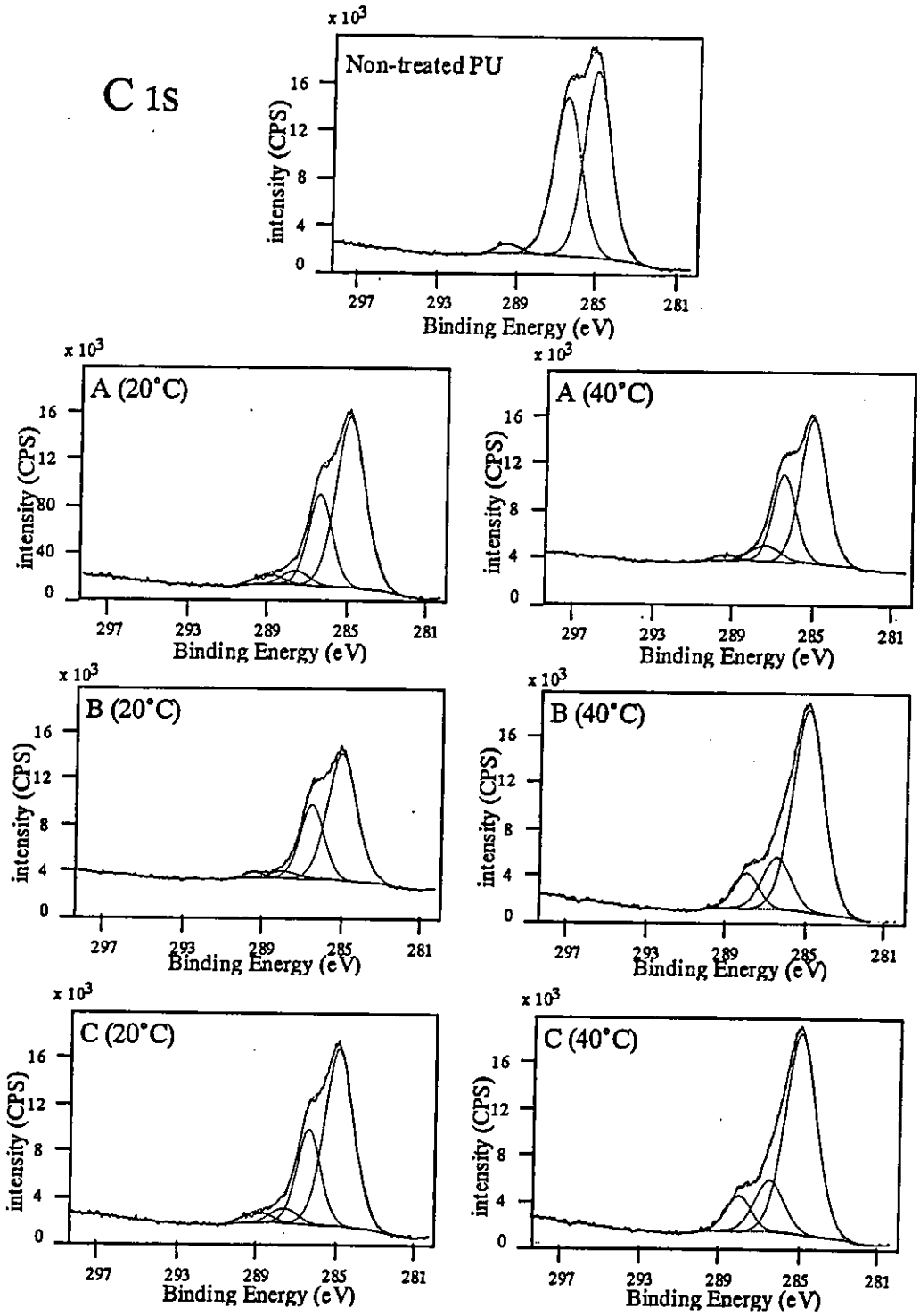

Figure 5. High-resolution C_{1S} spectra of segmented polyurethane with or without treatments of adsorption/desorption of PNIPAM–heparin with different mol wt of graft chains. The mol wt of graft chain; A (2×10^3 g/mol), B (1×10^4 g/mol), and C (1×10^5). Temperature denotes the washing temperature.

immersed in a 1% aqueous solution containing PNIPAM–heparin and incubated at either 20 or 40 °C for 30 min (adsorption step) and then subjected to washing with water at either 20 or 40 °C. The wettability and XPS measurements showed that adsorption of PNIPAM–heparin is enhanced at treatment temperatures above LCST (Table 3). That is, when the temperature at both the adsorption and washing steps was 20 °C, only a slight decrease in receding contact angle, a reduced O/C ratio, and an increased N/C ratio were observed. This is the same in the case of the adsorption temperature of 40 °C and washing temperature of 20 °C, indicating that adsorbed PNIPAM–heparins were removed from the surface although some of them remained. On the other hand, a markedly reduced receding angle, a decreased O/C ratio, and an increased N/C ratio, the last two of which approached the theoretical values of PNIPAM, were noted when the temperature at both steps was 40 °C. Therefore, it can be said that at a physiological temperature, PNIPAM–heparin is precipitated and remains on the surface.

Fluorescent images of samples subjected to adsorption and desorption (each step was carried out at 20 or 40 °C) were obtained as follows: first, immersion into albumin-